Applied Geochemistry 176 (2024) 106213

Contents lists available at ScienceDirect

Applied Geochemistry

journal homepage: www.elsevier.com/locate/apgeochem

Magmatic and rock-leaching contributions to the metal load in hydrothermal fluids at Þeistareykir, Iceland

Marion Saby [a,*], Vincent van Hinsberg [b], Daniele L. Pinti [a], Kim Berlo [b], Bjarni Gautason [c], Ásgerður Sigurðardóttir [d], M. Clara Castro [e]

[a] GEOTOP & Département des Sciences de la Terre et de l'atmosphère, Université du Québec à Montréal, 201 Av. du Président Kennedy, Montréal, Canada
[b] GEOTOP & Department of Earth and Planetary Sciences, McGill University, 3450, University Street, Montréal, Canada
[c] ÍSOR Iceland GeoSurvey, Orkugardur, Grensásvegur 9, Reykjavik, Iceland
[d] Landsvirkjun, Háaleitisbraut 68, Reykjavik, Iceland
[e] Department of Earth and Environmental Sciences, University of Michigan, Ann Arbor, USA

ARTICLE INFO

Editorial handling by: Orfan Shouakar-Stash

Keywords:
Volatile metals
Noble gases
Magma degassing
Water-rock interaction
Geothermal systems

ABSTRACT

Magmatic-hydrothermal systems are key environments to study the transfer of elements from the deep Earth to the surface and the mobilization and re-distribution of elements within the crust. These systems have been recognized as potential active analogue sites for ore deposition. The source of fluids and their metal load is split between the relative contributions from degassing of underlying magma and interactions between the hydrothermal fluid and the host rock. Here, we combine analyses of noble gases and volatile metals in fluids and rocks from the Þeistareykir geothermal field (NE Iceland) to provide constraints on the relative contribution of these two sources. Helium isotope data suggest 80–85% originated from magma degassing. The $^{3}He/^{4}He$ ratio, corrected for atmospheric contamination (Rc/Ra) correlates with volatile metal abundances in surface fluids and indicates that Bi and Hg are predominantly derived from magma degassing. It is also shown that the deep geothermal reservoir fluid is dominated by magmatic input, except for Mn, Fe, Co, Cu, Ti and V, using the elemental signature of magmatic degassing and water-rock interaction. The spatial variations in Rc/Ra and surface fluid volatile metal contents among the wells suggest an impact of the local and regional structures on the fluid's pathway from depth to surface.

1. Introduction

Crustal, convective hydrothermal systems are predominantly initiated by heat from magma bodies intruded at shallow crustal depths, often at 5–10 km. In these systems, hydrothermal (or, synonymously, "geothermal") aqueous fluids are a complex mixture of meteoric water, groundwater, sometimes seawater, and water exsolved from the melt (e.g., Giggenbach, 1992) either found under sub- or supercritical conditions (e.g., Chambefort and Stefansson, 2020). A gas phase can coexist with this aqueous phase, mainly formed by magmatic gases released by the melt (CO_2, H_2S, N_2, noble gases etc.) with a minor contribution from radiogenic gases produced within the crustal reservoir (e.g., ^{4}He, $^{40}Ar^{*}$; Pinti et al., 2019) and atmospheric gases introduced by meteoric recharge.

Metals can be introduced to the geothermal fluids by magmas and/or by the interaction and element exchange with reservoir rocks (Weiss et al., 1977; Hedenquist and Lowenstern, 1994). In some cases, these fluids and gases are emitted to the surface in fumaroles, hot springs, or, in more extreme examples, as crater lakes and acid rivers (Christenson and Wood, 1993; Varekamp et al., 2001). In extreme cases, the mobilization and redistribution of metals which take place in such systems can lead to ore formation, particularly porphyry Cu–Mo–W deposits and epithermal Ag–Au ores (Tosdal et al., 2009; Sillitoe, 2010; Hedenquist and Henley, 1985; Hedenquist et al., 1993, 1998; Tardani et al., 2024).

Numerous studies in the last 50 years focused on the origins of hydrothermal fluids and metals within these systems (see section 2 of this manuscript for a general review), yet the relative contribution of magma degassing and rock leaching to the metal content of magmatic-hydrothermal systems is a matter of debate. It is commonly assumed that most of the water circulating in high-temperature geothermal fields is of meteoric origin, but the same may not be true for their volatile and metal contents (e.g., Yardley and Bodnar, 2014 for a general review).

* Corresponding author.
E-mail address: marion.saby23@gmail.com (M. Saby).

https://doi.org/10.1016/j.apgeochem.2024.106213
Received 6 April 2024; Received in revised form 27 September 2024; Accepted 30 October 2024
Available online 31 October 2024

There is further consensus that the thermal energy driving the hydrothermal system is supplied by magma, and it is therefore reasonable to assume the magma also contributes to some extent to the metal content of the hydrothermal fluids, especially for the most volatile elements. However, it is unclear if the input of magmatic fluids dominates the composition of hydrothermal fluids or if the re-mobilization of metals from the host rock during water-rock interactions (WRI) is the dominant process. Both processes are implicated in the formation of ore deposits, especially porphyry and epithermal deposits (Bodnar, 1995; Sillitoe, 2010). Water-rock interaction can be favored by the availability of large volumes of meteoric water in system (10–100 times the volume of magmatic fluids; Norton, 1984) and by reservoir residence times for those fluids which can exceed thousand (e.g., Birkle et al., 2016; Stefánsson et al., 2017; Saby et al., 2020) or even million-year timescales (Pinti et al., 2019).

Noble gases (He, Ne, Ar, Kr and Xe) are chemically inert and rare in most terrestrial reservoirs, two characteristics which make them excellent tracers of geodynamic processes. This includes magma degassing since noble gases preferentially partition into the gas phase (e.g., Carroll and Draper, 1994). Noble gases, and particularly the helium isotopes ^{3}He and ^{4}He, have been pivotal in showing variable mantle, crustal and meteoric inputs of volatiles into magmatic-hydrothermal systems (e.g., Mazor and Truesdell, 1984; Stuart et al., 1995; Burnard et al., 1999; Sano and Fischer, 2013; Pinti et al., 2019). This is because the mantle, the crust and the atmosphere have distinct ^{3}He/^{4}He isotopic signatures, with mantle enriched in primordial ^{3}He compared to ^{4}He with respect to the atmosphere while the crust is dominated by U and Th-produced radiogenic ^{4}He. The expected ^{3}He/^{4}He ratio (R) in the convective depleted MORB-type mantle (or DMM) is essentially constant (Allègre et al., 1995) at 8 ± 1 times the atmospheric ratio ($Ra = 1.384 \times 10^{-6}$; Clarke et al., 1976). In regions affected by mantle plumes, the R/Ra ratio is much higher, with 43–45 being the highest R/Ra measured in the Miocene alkali basalts of NW Iceland (Breddam and Kurz, 2001) and the picritic basalts of Baffin Island (Stuart et al., 2003). In contrast, crustal fluids are dominated by ^{4}He, which is produced by α-decay of ^{235}U, ^{238}U and ^{232}Th contained in the crust with only little ^{3}He from neutron reaction with ^{6}Li (Ballentine and Burnard, 2002), resulting in an R/Ra typically in the range of 0.02–0.03 (e.g., Mamyrin and Tolstikhin, 1984). Finally, meteoric fluids exclusively contain atmospheric noble gases, which are dissolved at the recharge at solubility equilibrium (ASW or Air Saturated Water) and have a R/Ra of 1 (by definition).

Several studies have looked at noble gases as tracers of ore-forming fluids in fossil magmatic-hydrothermal-related ore deposits (e.g., Simmons et al., 1987; Stuart et al., 1995; Hu et al., 1998a,b; Burnard et al., 1999, 2004; Burnard and Polya, 2004; Landis and Rye, 2005; Manning and Hofstra, 2017; Wu et al., 2017), by analyzing these in fluid inclusions trapped in sulfides. Helium (and argon) isotopic compositions were pivotal in discriminating magmatic from crustal fluids involved in ore formation. Noble gases have also been combined with halogen contents in these inclusions (e.g., Kendrick et al., 2006), but the actual metal load could not be measured in these micro-fluid pockets. There are only a handful of studies where noble gases have been studied directly together with the metal load in hydrothermal fluids (e.g., Simmons et al., 1987, 2016) which makes applying those combined tools very promising for future field and experimental studies.

For the magma sourcing of metals, relative volatility or emanation coefficients (commonly expressed as the enrichment factor relative to solid magmatic deposits) indicate which elements are preferentially released (Zoller et al., 1983; Crowe et al., 1987; Hinkley, 1991, 1999), producing an elemental fingerprint for magma degassing. The highest enrichment factors are found for volatile metals (e.g., Hg, Bi, Cd, Te and Se) and ligands (Cl, S), and distinct differences are observed for different geotectonic settings with arc emissions particularly enriched in Sb, As and Pb while MORB/plume setting are more enriched in Te, Se and Tl (Mather et al., 2012; van Hinsberg et al., 2017; Edmonds et al., 2018). A similar compositional fingerprint can be determined for water-rock interaction from chemical characterization of a suite of progressively altered rocks (e.g. Libbey and Williams-Jones, 2016). A complication in differentiating the two processes is that WRI acts on hydrothermal-system reservoir rocks which are often magmatic in origin and derived from similar magma compositions than the magmatic heating source. Moreover, magmatic element volatility depends on the availability and concentrations of ligands, as do element solubility in hydrothermal fluids and leachability of the rocks, leading to cross-correlation between these processes.

Here, elemental and isotopic signatures of noble gases in geothermal fluids from the high-enthalpy þeistareykir geothermal field in NE Iceland are combined with a suite of trace metals with varying geochemical affinity to bring new constraints on the sources of fluids and metals in magmatic-hydrothermal systems. Fluids have been sampled both at the surface for all the wells, and at depth in one well at þeistareykir and one well at Krafla. Variably altered rock fragments recovered from the geothermal production wells were sampled to directly determine the water-rock interaction mass transfer. At the time of sampling, the þeistareykir geothermal field was in the initial phase of exploitation and this study thus allows chemistry of the geothermal fluids to be understood prior to exploitation-related changes to the original fluid signature. It is expected that this primary fluid pattern will be progressively lost as a result of phase segregation and boiling induced by exploitation and fluid re-injection, as it is the case in many geothermal fields the world over (see Pinti et al., 2013, 2019).

This is the first study where a full isotopic and compositional characterization of noble gases and metals in both fluids and reservoir rocks is available for the same hydrothermal system. The combination of these datasets permits direct insights into the contributions of magma degassing and water-rock interaction to the metal load of a basalt-hosted magmatic-hydrothermal system settled within a mid-ocean ridge environment.

2. Rock leaching VS. Magma degassing: a long-standing debate

What do magmas contribute to magmatic-hydrothermal systems, and what are the sources of volatiles and metals in the associated fluids? These questions have been the focus of many studies but are still debated and remain essentially unresolved. It is well-established that fluids released by magma are relatively enriched in metals compared to their host magma because of their preferential partitioning into the fluid phases (Hedenquist et al., 1993) and that these fluids, therefore, sequester the metals and inject them into the hydrothermal system. However, it is unclear if sufficient mass of metal can be liberated in this process to lead to the formation of an exploitable ore deposit (Yang and Scott, 2006). On the other hand, mass balance on altered rocks and their fresh counterparts commonly shows extensive metal re-mobilization, which has been linked to the elevated temperatures of the hydrothermal fluids and their high ligand (Cl^{-}, SO_4^{2-}) concentrations, which provide anions to create complexes with metals (Seward et al., 2014; Williams-Jones and Migdisov, 2014). Rock leaching thus appears to be an efficient mechanism for concentrating metals in hydrothermal fluids. The ligands (such as halogens) are dominantly derived from magma degassing (e.g., Aiuppa et al., 2009), and authors supporting host-rock leaching as the dominant metal source therefore still must invoke a degassing contribution (Hedenquist and Lowenstern, 1994).

The idea that the leaching of host rocks by hydrothermal fluids is the dominant metal concentration process in the crust is defended with a number of strong arguments. For example, the study of mid-ocean ridge (MOR) vents showed that the primary process involved in metal concentration is the interaction between seawater and basaltic crust with only a minor addition from magmatic fluids (Weiss et al., 1977; Tivey, 2007; Shanks and Thurston, 2012). Unlike MOR environments, felsic magmas often exsolve acid-volatile species (SO_2, HCl, HF), that can substantially lower the pH of the fluids circulating in the hydrothermal system and increase ligand concentrations. This changes the types of

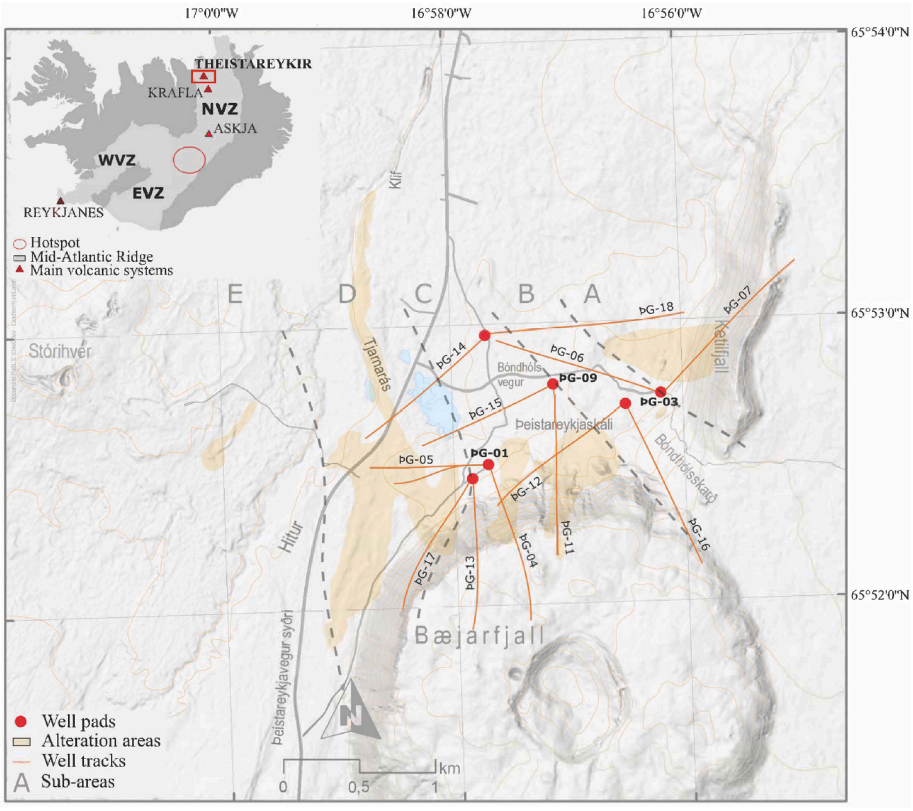

Fig. 1. A simplified map of the þeistareykir geothermal field with major alteration zones (E, D, C, B, A) and the positions of the sampled sites (wells) are indicated. The well tracks represent the direction of the well downhole (deviated) and their length (see map scale). Numbers on the X- and Y-axes indicate the latitudinal and longitudinal geographical coordinates, respectively, on the World Geodetic System 1984 (WGS84). NVZ = Northern Volcanic Zone; WVZ = Western Volcanic Zone; EVZ = Eastern Volcanic Zone.

crustal alteration that take place and enhances metal leaching and transport even more, making these systems also more predisposed to ore-deposit formation (Gamo et al., 1997, 2006; Gena et al., 2001; Yang and Scott, 2006; Tardani et al., 2024).

The boom in ore deposit exploration led to extensive studies of magmatic-hydrothermal systems associated with active volcanism as modern analogues of the equivalent fossil mineralized systems (Weissberg et al., 1979; Henley et al., 1984; Berger and Bethke, 1985; Krupp and Seward, 1987, 1990; Clark and Williams-Jones, 1990; Hedenquist et al., 1993; Barnes and Seward, 1997). Such studies showed that, unlike submarine systems, magmatic-hydrothermal systems in continental settings such as volcanic arcs are more influenced by magmatic fluids, possibly up to 25% in volume, due to the involvement of felsic magmas (Reeves et al., 2011). Increasingly, magmatic fluids are being considered as a source of metals (i.e. Cu, Zn, Ag and Au) in addition to what is possible to be sourced from rock leaching alone (e.g., Hedenquist and Lowenstern, 1994; Yang and Scott, 2006; 2006; Sun et al., 2004; Simmons and Brown, 2006). In addition to water and major volatile species (i.e. CO_2, SO_2, H_2S), volcanic gases contain up to 6 ppm Cu, 12 ppm Pb, 11 ppm Zn, 7 ppm Sn, 250 ppb Ag, and 24 ppb Au (e.g., Symonds et al., 1987; Hedenquist et al., 2018; Wahrenberger et al., 2002; Williams- Jones et al., 2002; Moune et al., 2006; Mather et al., 2012; Nadeau et al., 2016; van Hinsberg et al., 2017; Hedenquist et al., 2018; Lowenstern et al., 2018). These concentrations are still lower than those measured in fluid inclusions, which are considered the most direct source of data on ore-forming fluid composition in fossil mineralized systems. Still, volcanic gases represent the low-density vapor exsolved from such fluids, which explains the lower abundances of metals found in these vapors (Hedenquist and Lowenstern, 1994).

3. Geology of the area and geochemistry of fluids and altered rocks

þeistareykir is a high-enthalpy liquid-dominated field located in the Northern Volcanic Zone of Iceland (NVZ, Fig. 1), which is part of the northeastern branch of the Mid-Atlantic oceanic ridge. It is located around 30 km northwest of Krafla and Námafjall, which are among Iceland's older producing geothermal fields. The development of the þeistareykir geothermal field is recent and began with nine wells drilled between 2002 and 2011. Exploitation of the field began in 2017 with a total of 18 wells drilled to depths from 1723 *m* to 2799 *m*. The plant currently has two generating units of 45MWe, making þeistareykir the fourth largest station in Iceland in terms of generated power.

3.1. Geology

þeistareykir is a central volcano system (þeistareykjarbunga shield volcano) dissected by fissure swarms resulting from the interplay between the spreading of the NVZ rift, and the deformation caused by the WNW-ESE-oriented transform zone called the Tjörnes Fracture Zone (TFZ; Khodayar et al., 2018). Volcanism is characterized by a series of olivine-tholeiitic and picritic basalt lava flows, mainly erupted from the þeistareykjarbunga volcano: Skildingahraun (>14.5 ka) lava shield; Stóravíti, a widespread (30 km^3) post-glacial lava shield that erupted approximately 10.5 ka ago (MacLennan et al., 2002); the picritic basalt Borgarhraun (10–8 ka); and the youngest þeistareykjahraun lava shield (2.4 ka) (Saemundsson, 2007).

The heat source of the geothermal field has been related to the most recent mafic volcanic activity in the area (the 2.4 ka old þeistareykjahraun basaltic eruption), and the distribution of fumaroles suggests that it is supplied by an *E*-W-oriented magmatic intrusion, likely of

basaltic nature (Óskarsson et al., 2013). The radiogenic isotope (Sr, Nd, Hf, Pb) and major and trace element compositions of the erupted basalts are little affected by crystal fractionation and are essentially unaffected by interaction with the crust (Stracke et al., 2003). The þeistareykir basalts are therefore thought to be relatively close in composition to primary melts from the mantle (Stracke et al., 2003). Volcanic reservoir rocks at depth are thought to be compositionally equivalent to the surface exposures with variable alteration owing to water-rock interaction in the geothermal reservoir.

The surface area corresponding to the full extension of the þeistareykir hydrothermal system is 25–30 km^2. Still, surface manifestations are confined to the eastern part of the fissure swarm, northwest and north of Mt. Bæjarfjall, over an area of 11 km^2 (Kristinsson et al., 2013, Fig. 1). The þeistareykir thermal area has historically been divided into five *N*–S oriented sub-areas, which from east to west are: Ketilfjall (A), Bóndhólsskard (B), þeistareykjagrundir (C), Tjarnarás (D), and þeistareykjahraun (E) (Fig. 1). These areal subdivisions are based on the reservoir temperatures estimated by gas geothermometry, ranging from 100 °C for area C and E to 330 °C for areas A and D (Ármannsson et al., 1986). Among these areas, Ketilfjall (A), þeistareykjagrundir (C), and Tjarnarás (D) were regarded as more promising for drilling.

3.2. Fluid chemical composition

Between 2002 and 2017, 18 wells were drilled. The eleven wells studied here range from 1824 *m* for the well þG-11 to 2799 *m* for the well þG-06. All the wells are deviated except for the vertical wells þG-01, þG-03, and þG-09. More details on the wells can be found in Saby et al. (2020, 2022).

Based on stable isotopes (δ^2H, $\delta^{18}O$) of water, noble gas isotopes, and $^{87}Sr/^{86}Sr$ ratios, four fluid sources were identified in the geothermal field: 1) modern, local meteoric water; 2) sub-modern meteoric (glacial) water from regional highlands precipitation; 3) pre-Holocene glaciated meteoric water, characterized by strongly depleted δ^2H values and calculated U–Th/He and K–Ar fluid residence times from 57 ± 20 ka to 160 ± 80 ka; and, finally, 4) a ^3He-enriched magmatic fluid (Stefánsson et al., 2017; Sveinbjörnsdóttir et al., 2013, 2015; Saby et al., 2020; Pinti et al., 2022).

Na–K–Cl dominates the geochemistry of the production well fluids sampled at the surface with a TDS of about 350 mg/l. Chlorine content varies from 5.4 to 173 ppm while SO_4 varies from 0.7 to 33 ppm. The Na/Cl ratio is higher in well fluids than in fluids from natural surface manifestations. The fluids sampled at the wellhead exhibit a near-neutral pH, while fluids directly sampled at depth during well shut-in showed an acidic pH of ca. 2.5 (Saby et al., 2022). This is regarded to be a result of shutting in the well and reflecting mixing between deep near-neutral fluids with a shallow inflow of fluids that have been acidified by condensation of volcanic H_2S in the water phase of the upper part of the system (see Saby et al., 2022). Trace metals are significantly diluted in surface fluids (both at the wellhead and in hot springs) compared to deep fluids (Saby et al., 2022). In the water phase, H_2S is the dominant gas, with contents ranging from 31 to 88 ppm, followed by CO_2, with contents ranging from 9.4 to 62 ppm. In the steam phase, the dominant gas is CO_2, with contents ranging from 285 to 5597 ppm, followed by H_2S, with contents ranging from 207 to 1141 ppm. Nitrogen in the dry gas phase (vapor phase minus the steam) vary from 1.6 to 46 ppm. The highest gas concentrations measured in wells (CO_2 = 24,723 ppm, H_2S = 4673 ppm, H_2 = 122.1 ppm, CH_4 = 149.03 ppm) are found in the Ketilfjall (A) and Tjarnarás (D) areas, and at least in Tjarnarás is probably due to subsurface steam condensation, as suggested by Darling and Ármannsson (1989).

Although gas measurements in þeistareykir have been undertaken for over half a century (Hermannsson and Líndal, 1951), noble gas data remained scarce and mainly limited to sampling from natural surface manifestations (Hilton et al., 1990; Poreda and Arnórsson, 1992; Füri et al., 2010), since þeistareykir wells were drilled only recently. Volatiles from the NVZ have been mainly sourced from the depleted upper mantle based on the work of Hilton et al. (1990), who measured R/Ra values from 6.9 to 9.4 in fluids, and that of Breddam et al. (2000), who measured R/Ra values of 7.99–9.75 in picrites of þeistareykir. Both set of values are close the R/Ra = 8 ± 1 value of the DMM (e.g., Allègre et al., 1995). Successive work by Füri et al. (2010) showed slightly higher values up to 10.7 in fumaroles of nearby Námafjall and Krafla geothermal fields, and Saby et al. (2020) calculated a R/Ra endmember value for the þeistareykir magmatic fluid of 11.45 (Table A1). This suggests that even if the DMM source is dominating the release of volatiles in the region, *ca.* 10% of helium could be derived from the Icelandic mantle plume, which shows R/Ra values of 42–45 (Breddam et al., 2000). The other noble gases from the þeistareykir well fluids mainly show an atmospheric signature with the mantle signal obliterated by the meteoric water the dominant fluid component in most Icelandic geothermal fields (e.g., Stefánsson et al., 2017). Only argon shows a clear but small terrigenic (either mantle and/or crustal) component with measured $^{40}Ar/^{36}Ar$ ratios ranging from 298.8 to 307.3 (Saby et al., 2020).

3.3. Secondary mineralogy of reservoir rocks

Extensive research has been conducted on the secondary mineralogy in the þeistareykir geothermal field based on petrography of cuttings from the wells. Secondary minerals found in well's cuttings of the þeistareykir geothermal reservoir are characteristic of prolonged water-rock interactions at high temperatures between 200 °C and 350 °C (Gundfinnsson, 2014). Quartz and the zeolite mineral wairakite ($CaAl_2Si_4O_{12}{\cdot}2H_2O$) are found at less than 100 *m* depth in wells þG-07, þG-03 and þG-06, suggesting that the temperature was at least 200 °C at some point at this depth. Then at 342 *m*, prehnite is seen in þG-07, indicating a temperature of at least 240 °C. Actinolite appears at about 750 *m* in þG-07, þG-03 and þG-06, at which point, the temperature should have reached at least 280 °C. Traces of hornblende found in þG-03 and þG-06 below 2300 *m* suggest that the maximum temperature in this part of the geothermal reservoir is about 350 °C (Gundfinnsson, 2014). Studies of fluid inclusions in the lower part of þG-03 show a range of temperatures, exceeding 350 °C at the high end. These results agree with downhole logging after the well drilling that recorded over 350 °C in the deepest part. Traces of hydrothermal calcite can be found at almost all depths in well þG-03 down to the bottom. In contrast, calcite is sporadic in the lower part of þG-06 and is absent in well þG-07 in the 1400–1700 *m* range (Gundfinnsson, 2014). Wells þG-04 and þG-05, located close to Bæjarfjall mountain, 1 km to the ENE of þG-07, þG-03, and þG-06, show that the high-temperature alteration is equally shallow, with quartz, wairakite, chlorite, epidote, and prehnite all present in the shallowest sample from 310 *m*. Actinolite first appears between 500 and 600 *m* and calcite is not seen below 800–900 *m* in either of the two wells. Thus, it is likely that the temperature in the part of the reservoir penetrated by þG-04 and þG-05 exceeds 280–300 °C. Accessory phases are present and include sulfides and oxides but were not studied in detail by Gundfinnsson (2014).

4. Analytical methods

4.1. Noble gas sampling and analyses

A total of 11 geothermal wells (þG-01, þG-03, þG-04, þG-05, þG-06, þG-07, þG-11, þG-12, þG-13, þG-16, þG-17, see Fig. 1) were sampled for analysis of noble gases in the vapor phase and the full suite of major and trace elements in the liquid phase). Deep fluid samples were collected from wells þG-01 (þeistareykir) and K-21 (Krafla) at depths of 850 m (K-21) and 1420 and 1600 m (þG-01), using the in-situ Ti-sampler developed by Brown and Simmons (2003). Details regarding deep fluids sampling and analysis can be found in Saby et al. (2022). Water and gas phases were also collected directly at the wellhead using a portable

Table 1
Chemical composition of the surface fluids at the Þeistareykir geothermal field.

Elements (ppm)	ÞG-01	±	ÞG-03	±	ÞG-04	±	ÞG-05	±	ÞG-06	±	ÞG-07	±	ÞG-11	±	ÞG-12	±	ÞG-13	±	ÞG-16	±	ÞG-17	±
Cl	96.26	2.00	80.20	1.67	59.71	1.24	61.08	1.27	173.03	3.60	18.52	0.38	5.39	0.11	86.88	1.81	70.94	1.47	52.53	1.09	85.09	1.768
SO4	12.17	0.20	10.21	0.17	1.27	0.02	33.31	0.55	2.94	0.05	9.63	0.16	0.69	0.01	7.12	0.12	2.79	0.05	9.70	0.16	2.81	0.046
Li	0.12	*n.d.*	0.07	*n.d.*	0.18	*n.d.*	0.14	*n.d.*	0.27	*n.d.*	0.14	*n.d.*	0.09	*n.d.*	0.16	*n.d.*	0.24	*n.d.*	0.20	*n.d.*	0.15	*n.d.*
Na	107.10	10.00	130.93	12.22	59.65	5.57	128.92	12.04	127.66	11.92	91.45	8.54	31.97	2.98	220.21	20.56	124.20	11.60	83.28	7.78	89.61	8.366
K	21.84	1.60	27.98	2.05	13.13	0.96	22.64	1.66	28.49	2.09	18.51	1.36	6.53	0.48	23.01	1.69	25.15	1.84	20.33	1.49	19.89	1.457
Mg	0.03	*n.d.*	0.01	*n.d.*	0.02	*n.d.*	0.00	*n.d.*	0.01	*n.d.*	0.01	*n.d.*	0.0010	*n.d.*	0.01	*n.d.*	0.01	*n.d.*	0.01	*n.d.*	0.01	*n.d.*
Ca	0.23	*n.d.*	0.23	*n.d.*	0.06	*n.d.*	0.46	*n.d.*	0.22	*n.d.*	0.25	*n.d.*	0.01	*n.d.*	0.28	*n.d.*	0.10	*n.d.*	0.37	*n.d.*	0.12	*n.d.*
Sr	0.01	*n.d.*	0.01	*n.d.*	0.002	*n.d.*	0.002	*n.d.*	0.004	*n.d.*	0.01	*n.d.*	*n.d.*	*n.d.*	0.002	*n.d.*	0.002	*n.d.*	0.001	*n.d.*	0.001	*n.d.*
Ba	0.00012	0.024	0.00039	0.08007	0.00073	0.15062	0.00078	0.16179	0.00052	0.10655	0.00023	0.04676	0.00013	0.02710	0.00043	0.08938	0.00059	0.12166	0.00048	0.09972	0.00026	0.053
V	0.003	0.630	0.004	0.725	0.000	0.068	0.006	1.128	0.005	0.954	0.004	0.788	0.002	0.356	0.010	1.856	0.003	0.619	0.015	2.759	0.002	0.431
Cr	0.00002	*n.d.*	0.00001	*n.d.*	0.00008	*n.d.*	0.00005	*n.d.*	0.00001	*n.d.*	0.00002	*n.d.*	0.00009	*n.d.*	0.00002	*n.d.*	0.00001	*n.d.*	0.00002	*n.d.*	0.00003	*n.d.*
Mn	0.002	0.083	0.001	0.042	0.001	0.042	0.363	15.065	0.001	0.042	0.001	0.042	0.001	0.042	*n.d.*	*n.d.*	*n.d.*	*n.d.*	0.001	0.042	0.001	0.042
Fe	0.003	0.001	0.007	*n.d.*	0.023	*n.d.*	0.008	*n.d.*	0.005	*n.d.*	0.004	*n.d.*	0.010	*n.d.*	0.011	*n.d.*	0.003	*n.d.*	0.002	*n.d.*	0.005	*n.d.*
Co	0.00003	*n.d.*	*n.d.*	*n.d.*	0.00002	*n.d.*	*n.d.*	*n.d.*	*n.d.*	*n.d.*	*n.d.*	*n.d.*	*n.d.*	*n.d.*	*n.d.*	*n.d.*	*n.d.*	*n.d.*	*n.d.*	*n.d.*	*n.d.*	*n.d.*
Ni	0.0002	0.0360	*n.d.*	*n.d.*	0.0001	0.0253	*n.d.*	*n.d.*	0.0001	0.0111	0.0001	0.0134	0.0001	0.0236	0.0001	0.0130	*n.d.*	*n.d.*	0.0001	0.0117	*n.d.*	*n.d.*
Cu	0.002	*n.d.*	0.001	*n.d.*	0.001	*n.d.*	*n.d.*	*n.d.*	0.001	*n.d.*	0.00044	*n.d.*	*n.d.*	*n.d.*	0.002	*n.d.*	0.001	*n.d.*	0.00048	*n.d.*	0.001	*n.d.*
Zn	0.002	*n.d.*	0.001	*n.d.*	0.001	*n.d.*	0.003	*n.d.*	0.001	*n.d.*	0.001	*n.d.*	0.00023	*n.d.*	0.001	*n.d.*	0.001	*n.d.*	0.007	*n.d.*	0.001	*n.d.*
Mo	0.001	0.230	0.001	0.164	0.008	1.792	0.000	0.075	0.022	4.945	0.00024	0.054	0.00013	0.029	0.028	6.440	0.00030	0.069	0.001	0.239	0.005	1.049
Cd	0.000024	2.131300	0.000026	3.017433	0.000029	3.426533	0.000025	6.598673	0.000028	1.714468	0.000025	5.470696	*n.d.*	*n.d.*	0.000028	1.715321	0.000025	3.33	0.000027	2.405336	0.000025	2.037
Hg	0.00015	2.061	0.00019	1.856	0.00007	0.390	0.00010	0.717	0.00016	0.933	0.00011	0.549	*n.d.*	*n.d.*	0.00011	1.650	0.00009	0.494	0.00013	0.276	0.00011	1.784
Al	1.78	229.00	2.86	367.94	2.31	297.19	1.67	214.85	1.32	169.82	1.61	207.13	2.70	347.36	0.94	120.55	1.99	256	2.96	380.81	2.34	301.045
Sb	0.000005	7.722772	0.000008	0.558717	0.001160	0.412083	0.000224	0.790076	0.000051	1.071254	0.000008	1.467815	*n.d.*	*n.d.*	0.000820	0.534445	0.000075	1.12	0.000034	2.805291	0.000197	2.618
Tl	0.000038	0.797	0.000083	0.615	0.000039	0.481	0.000076	0.595	0.000089	0.213	0.000041	0.541	*n.d.*	*n.d.*	0.000048	0.726	0.000073	0.364	0.000054	0.305	0.000069	0.418
Bi	0.000024	3.811	0.000042	3.809	0.000017	2.724	0.000020	2.237	0.000023	2.528	0.000020	2.083	*n.d.*	*n.d.*	0.000015	2.403	0.000019	1.929	0.000019	2.457	0.000012	13.608
B	1.15	*n.d.*	0.000042	*n.d.*	0.000017	*n.d.*	0.000020	*n.d.*	0.000023	*n.d.*	0.000020	*n.d.*	*n.d.*	*n.d.*	0.000015	*n.d.*	0.000019	*n.d.*	0.000019	*n.d.*	0.000012	*n.d.*
Si	351	24	474	32	310	21	251	17	516	35	364	25	248	17	496	34	397	27	465	32	419	29
As	0.003	0.510	0.030	0.481	0.130	0.079	0.000406	0.552	0.045	0.262	0.027	0.167	0.005	0.96	0.230	0.740	0.005	0.294	0.002	0.101	0.009	0.416

n.d. not determined.

Table 2
Chemical composition of the fresh rocks at the Þeistareykir geothermal field.

Elements	ROC-1	±	ROC-3	±	ROC-4	±	ROC-5	±	ROC-6	±	ROC-7	±	ROC-8	±	ROC-9	±	ROC-11	±	ROC-12	±	ROC-13	±	ROC-15	±
wt%																								
SiO2	58.99	1.82	42.69	1.53	54.73	1.74	44.02	1.55	53.64	1.72	40.77	1.49	40.16	1.48	44.15	1.55	42.34	1.52	57.78	1.80	42.37	1.52	58.29	1.81
TiO2	1.21	0.04	0.56	0.03	0.72	0.03	0.88	0.03	0.43	0.03	0.29	0.02	0.39	0.03	1.00	0.03	0.95	0.03	0.87	0.03	0.73	0.03	0.84	0.03
Al2O3	31.95	6.29	15.53	4.49	26.92	5.74	17.64	4.72	23.80	5.40	11.16	4.01	14.05	4.33	16.27	4.57	15.10	4.44	31.84	6.28	16.82	4.63	33.44	6.46
FeO	10.62	0.11	8.63	0.09	9.42	0.09	9.38	0.09	8.52	0.08	8.28	0.08	8.30	0.08	10.32	0.10	9.64	0.10	10.31	0.10	7.69	0.08	8.53	0.08
MnO	0.21	0.01	0.16	0.01	0.18	0.01	0.18	0.01	0.16	0.01	0.15	0.01	0.14	0.01	0.19	0.01	0.18	0.01	0.19	0.01	0.14	0.01	0.16	0.01
CaO	13.08	0.20	11.71	0.18	12.96	0.20	12.25	0.19	11.19	0.17	9.19	0.14	9.98	0.15	11.17	0.17	11.55	0.18	12.40	0.19	12.81	0.20	14.81	0.23
K2O	0.17	0.02	0.10	0.02	0.10	0.02	0.14	0.02	0.10	0.02	0.10	0.02	0.10	0.02	0.16	0.02	0.14	0.02	0.16	0.02	0.11	0.02	0.10	0.02
ppm																								
Li	3.91	5.10	2.65	4.96	3.25	6.60	3.26	19.86	2.34	3.62	2.15	9.70	2.26	4.91	3.25	6.29	3.33	7.37	3.55	6.54	2.37	6.39	3.24	6.61
Na	15876.90	0.87	9763.28	11.82	11600.22	9.96	12045.60	20.03	8206.32	4.98	6597.26	13.69	6913.11	6.75	13127.24	9.95	13492.58	5.26	13714.75	7.79	11805.97	5.21	14271.26	5.44
K	1007.88	0.81	369.01	12.32	522.15	9.08	721.20	18.89	164.40	5.11	115.77	16.58	133.04	6.08	964.74	7.61	808.71	7.64	1026.46	6.34	495.80	6.70	481.14	4.31
Rb	2.24	7.12	0.71	12.47	1.02	7.59	1.41	18.90	0.36	7.04	0.23	20.22	0.30	8.76	2.03	6.71	1.65	7.45	2.38	6.81	1.14	7.29	0.96	3.42
Cs	0.02	0.65	0.01	1.95	0.01	2.12	0.02	2.85	0.00	2.05	0.00	1.35	0.00	3.63	0.03	3.52	0.02	3.66	0.03	1.43	0.01	2.93	0.01	4.67
Mg	47738.05	4.10	75299.11	5.55	74189.42	8.56	52984.33	15.99	131270.10	5.66	126781.19	11.61	123940.51	6.90	43453.66	4.94	40808.50	3.41	53113.52	4.99	43023.41	5.46	54311.14	8.46
Ca	105108.64	2.66	87229.56	6.56	96993.62	8.70	88813.01	11.52	80423.34	5.77	62920.31	10.54	69200.27	6.24	82927.94	6.43	90602.23	3.14	90941.82	6.17	102275.59	5.38	121067.38	4.85
Sr	161.90	0.80	81.62	9.70	98.20	9.44	101.87	10.61	52.11	5.38	40.10	10.78	44.12	5.57	124.33	8.80	133.50	3.24	139.85	6.51	130.32	5.25	150.38	3.84
Ba	42.52	3.20	13.41	11.27	18.59	9.00	24.48	12.49	6.64	4.40	4.31	10.74	5.71	8.25	33.86	8.17	29.08	5.50	40.10	6.20	23.28	7.06	21.93	2.16
Ti	7260.54	7.17	3124.74	3.63	4303.43	7.39	5131.12	20.59	2564.81	4.78	2089.75	9.74	2310.14	6.39	6045.79	4.65	5411.84	9.54	5231.99	4.53	3507.86	19.95	5043.93	17.03
V	360.95	3.45	231.83	4.33	255.71	9.03	286.29	26.64	196.50	5.31	160.06	12.14	170.30	6.62	307.58	2.92	278.19	7.63	287.34	4.15	213.90	7.28	276.89	11.49
Cr	97.53	4.25	1070.77	5.76	987.20	9.70	406.04	24.29	2384.31	4.68	2138.46	12.36	2102.60	7.07	96.11	6.37	85.92	2.62	87.95	5.75	218.26	3.92	269.53	8.26
Mn	1725.37	3.38	1272.34	5.24	1408.13	9.29	1393.50	19.18	1339.98	5.63	1190.30	12.19	1228.73	5.58	1474.60	3.42	1368.19	4.54	1570.47	4.87	1122.12	7.22	1453.46	9.45
Fe	94498.72	3.84	69953.52	5.07	78814.64	8.98	78878.70	20.32	76758.47	5.48	69497.95	12.26	69176.15	5.59	82796.90	1.47	74952.57	6.95	88572.76	5.10	59361.83	9.05	77918.36	11.80
Co	58.39	2.50	60.15	5.96	62.88	8.42	55.14	22.57	84.75	5.20	87.22	11.88	80.94	6.19	52.98	4.08	49.30	6.55	61.37	6.50	45.79	8.40	57.09	8.85
Ni	69.81	1.96	310.01	7.60	277.72	8.99	142.08	21.28	751.14	6.10	773.92	12.51	683.27	5.74	72.54	6.83	65.23	6.03	91.66	6.36	85.26	6.25	105.95	8.89
Cu	133.68	11.70	86.69	9.78	110.41	7.94	116.03	19.56	96.03	3.41	58.86	13.70	69.51	3.47	372.49	9.64	115.12	12.02	108.18	5.41	59.57	10.19	136.18	8.40
Zn	98.36	3.97	78.09	1.93	81.94	6.59	80.50	12.99	77.49	4.74	67.74	10.98	62.98	3.31	85.83	0.99	73.34	6.33	85.95	2.79	62.28	10.90	79.62	10.44
Zr	58.34	8.87	23.57	4.19	31.98	6.48	37.58	12.23	17.97	3.36	14.65	11.27	17.04	6.96	46.86	4.22	41.76	4.17	43.28	3.51	31.07	12.60	42.37	8.49
Nb	3.99	11.46	1.09	8.09	1.77	6.24	3.13	20.97	0.56	5.83	0.51	9.81	0.45	6.92	3.24	2.96	2.84	6.36	3.54	4.20	1.52	23.16	2.22	16.68
Mo	0.34	8.36	0.16	4.94	0.23	6.15	0.31	13.08	0.12	2.90	0.79	13.53	0.14	8.21	0.31	4.44	0.27	4.03	0.33	2.82	0.17	11.89	0.23	8.68
Ag	0.03	17.23	0.02	13.49	0.02	11.63	0.03	10.67	0.02	8.66	0.02	18.09	0.01	16.16	0.03	6.36	0.02	10.52	0.03	5.29	0.02	14.74	0.03	4.73
Cd	0.11	3.65	0.12	8.79	0.12	4.53	0.09	1.47	0.09	20.40	0.07	21.46	0.07	5.86	0.09	9.99	0.08	22.79	0.08	3.57	0.13	3.10	0.10	5.64
Hf	1.67	6.23	0.72	2.71	0.90	7.54	0.99	12.65	0.55	5.61	0.46	10.80	0.53	4.85	1.29	4.49	1.15	5.13	1.14	2.90	0.88	11.67	1.19	11.32
Ta	0.50	13.53	0.31	8.62	0.36	13.61	0.41	5.42	0.34	18.90	0.54	13.42	0.46	13.89	0.50	5.04	0.42	4.44	0.52	10.73	0.33	25.97	0.49	11.56
W	5.32	16.27	6.50	8.62	5.68	12.94	4.37	11.92	7.77	5.76	11.71	12.94	9.54	10.52	5.48	5.60	6.11	1.07	5.49	5.58	4.45	25.26	6.38	15.52
Hg	0.03	7.15	0.03	4.74	0.03	8.06	0.03	10.95	0.04	1.68	0.05	12.47	0.04	7.24	0.03	4.78	0.03	1.44	0.03	3.49	0.03	10.81	0.04	8.87
Al	87412.00	0.18	61591.84	8.91	72702.58	8.74	71682.81	11.48	57382.35	5.93	44438.66	10.40	49900.63	5.76	66730.00	8.16	78456.57	3.20	80693.10	6.37	89008.84	5.17	103651.71	3.77
Ga	9.28	1.93	6.06	9.88	6.82	9.94	6.89	18.06	5.00	5.95	4.16	11.65	4.14	6.29	7.55	8.19	7.53	4.45	7.92	5.94	6.81	7.87	8.24	4.46
In	0.06	4.45	0.04	8.31	0.04	15.26	0.04	27.00	0.03	9.29	0.03	14.02	0.03	11.43	0.05	6.42	0.05	3.22	0.05	6.08	0.04	8.09	0.05	10.62
Sn	0.67	12.62	0.32	7.48	0.54	25.50	0.42	19.93	0.26	0.95	0.35	26.46	0.22	4.82	0.53	3.37	0.53	5.18	0.47	7.10	0.35	21.62	0.47	8.00
Sb	0.02	6.13	0.01	13.17	0.02	3.27	0.02	5.86	0.01	4.99	0.01	23.69	0.01	4.71	0.01	11.11	0.01	8.98	0.02	2.38	0.02	10.90	0.01	3.78
Tl	0.01	7.11	0.01	16.10	0.00	7.27	0.01	8.16	0.00	10.26	0.00	11.50	0.00	6.20	0.01	8.44	0.00	5.35	0.01	8.67	0.01	6.49	0.00	1.69
Pb	5.08	10.63	6.06	18.25	5.88	10.59	4.97	15.33	6.13	5.25	5.50	14.95	5.10	6.22	5.02	12.91	4.11	8.92	5.18	7.81	5.96	12.00	7.26	5.47
Bi	0.02	5.65	0.02	11.82	0.01	8.92	0.03	20.85	0.01	15.88	0.01	12.63	0.48	6.98	0.02	8.09	0.01	5.03	0.01	13.99	0.01	5.31	0.01	6.86
Si	248118.06	1.34	210652.18	6.48	222075.11	7.14	205768.23	11.09	218088.97	4.51	190587.76	9.11	196365.07	4.99	204132.15	6.42	207968.33	2.93	224948.50	5.02	217017.51	4.33	254957.92	3.91
As	0.09	6.01	0.06	5.76	0.07	11.64	0.08	13.02	0.03	16.19	0.04	24.01	0.03	12.19	0.10	7.67	0.10	8.91	0.11	10.56	0.07	14.34	0.09	11.36
Se	0.07	20.78	0.08	40.69	0.10	18.82	0.10	30.37	0.08	2.55	0.07	10.03	0.07	35.08	0.16	4.60	0.07	7.08	0.13	22.37	0.07	27.89	0.10	26.36
Sc	44.38	4.51	33.15	3.99	37.30	7.69	35.77	10.87	33.16	6.30	26.31	9.49	28.93	5.15	36.75	4.54	35.95	2.93	40.41	4.04	33.34	4.50	42.06	8.02
Y	22.93	4.61	13.01	4.64	16.06	6.72	16.07	10.04	11.57	4.92	9.30	9.71	10.51	5.16	18.45	4.26	17.05	3.77	17.14	3.96	14.32	6.85	18.85	5.50
La	3.88	9.58	1.26	10.75	1.83	7.47	2.47	12.15	0.62	2.28	0.47	12.06	0.54	5.56	3.04	5.84	2.68	4.02	3.16	3.65	1.90	4.88	2.29	1.03
Ce	10.35	8.80	3.81	10.61	5.23	8.22	6.54	15.45	2.10	2.90	1.66	12.86	1.84	1.49	8.37	6.52	7.21	4.71	7.91	5.07	5.39	6.49	6.65	1.84
Pr	1.58	8.00	0.60	9.41	0.83	7.74	0.98	14.87	0.37	2.99	0.30	11.20	0.33	1.66	1.26	6.10	1.12	3.36	1.18	4.76	0.86	6.59	1.08	3.06
Nd	7.97	8.95	3.29	8.34	4.34	7.99	4.90	12.59	2.16	3.27	1.75	9.50	1.92	3.26	6.32	6.00	5.76	3.13	5.79	4.04	4.48	5.70	5.72	3.53
Sm	2.65	7.99	1.23	5.23	1.55	8.09	1.64	12.31	0.94	3.01	0.75	10.26	0.84	3.33	2.08	5.97	1.88	4.53	1.84	3.06	1.58	6.67	2.04	4.81

(*continued on next page*)

Table 2 (*continued*)

Elements	ROC-1	±	ROC-3	±	ROC-4	±	ROC-5	±	ROC-6	±	ROC-7	±	ROC-8	±	ROC-9	±	ROC-11	±	ROC-12	±	ROC-13	±	ROC-15	±
Eu	1.08	2.66	0.52	7.48	0.64	8.90	0.65	12.04	0.39	5.07	0.31	11.55	0.36	6.53	0.82	6.54	0.77	3.42	0.75	4.24	0.67	5.84	0.86	4.11
Gd	3.19	6.74	1.62	6.18	2.00	6.97	2.03	10.73	1.30	2.32	1.07	12.00	1.17	4.96	2.49	5.11	2.25	4.38	2.22	4.39	1.93	6.84	2.52	6.09
Tb	0.62	5.87	0.33	3.76	0.40	6.54	0.39	11.09	0.28	3.45	0.23	10.68	0.26	4.78	0.48	4.49	0.44	4.70	0.42	4.65	0.38	4.12	0.50	6.23
Dy	4.07	5.22	2.23	5.67	2.72	7.91	2.61	10.62	1.92	4.20	1.56	10.19	1.77	6.05	3.18	4.75	2.92	3.08	2.85	3.32	2.47	6.70	3.31	6.46
Ho	0.90	5.39	0.50	3.88	0.60	7.90	0.56	11.05	0.43	4.49	0.35	10.89	0.40	6.29	0.69	6.14	0.63	3.49	0.63	3.37	0.54	7.39	0.73	6.60
Er	2.48	5.08	1.43	4.21	1.71	8.06	1.61	12.93	1.24	4.71	1.01	9.61	1.16	4.93	1.95	4.32	1.78	3.17	1.77	4.92	1.56	7.36	2.05	5.30
Tm	0.38	4.84	0.22	3.84	0.26	7.76	0.25	8.45	0.19	6.31	0.16	12.41	0.18	4.32	0.30	4.84	0.27	2.83	0.27	3.06	0.24	5.01	0.31	6.00
Yb	2.55	5.13	1.48	3.60	1.72	7.61	1.66	9.93	1.30	3.62	1.05	10.81	1.18	5.13	1.98	3.57	1.81	5.21	1.83	2.68	1.57	6.58	2.07	6.34
Lu	0.38	6.68	0.22	3.34	0.26	7.93	0.25	12.08	0.19	4.93	0.16	11.26	0.18	5.39	0.29	5.66	0.27	4.11	0.28	3.83	0.23	5.23	0.31	7.60
Th	0.26	11.92	0.07	10.57	0.20	33.46	0.15	8.44	0.04	6.24	0.02	24.67	0.03	4.02	0.21	5.40	0.17	5.19	0.24	2.43	0.13	1.06	0.13	0.00
U	0.08	11.09	0.03	9.51	0.03	7.21	0.05	17.05	0.01	6.22	0.01	30.46	0.01	16.61	0.07	5.00	0.05	6.75	0.07	5.10	0.03	6.20	0.04	4.73

steam/fluid separator. Noble gases were collected using a standard refrigeration-grade 3/8") copper tube (14 cm^3 internal volume directly installed at the gas exit of the portable fluid/steam separator. After letting the gas flow for several minutes, the tubes were sealed using stainless steel pinch-off clamps. Helium isotopic ratios were measured in the recovered gas phase at the Noble Gas Laboratory, University of Michigan (UMICH) by using a Thermo Helix SFT, except for well þG -17, which was analyzed in the Noble Gas Laboratory of Geotop, using a Thermo Helix MC. In both institutions, gases were purified by gettering on Ti-sponges and/or ST-707 alloys and then He was separated from the other noble gases using a cryogenic trap. At UMICH, ^3He was measured using an electron multiplier in ion counting mode and ^4He on a Faraday cup. At Geotop, ^3He was measured by ion counting on the axial Compact Discrete Dynode™ (CDD) detector, while ^4He was determined on the axial Faraday cup. Typical blanks for He are 0.01–0.04%. Quantitative analyses were obtained by calibrating the two mass spectrometers with a known aliquot of standard air, with typical standard reproducibility for ^4He of 0.5–1% (see Saby et al., 2020 for details).

4.2. Major and trace metals analyses in water and rocks

After collection at the wellhead, the fluids sampled were divided into two sub-samples stored in pre-cleaned HDPE bottles: (1) an unacidified aliquot for the analysis of anions, (2) a sample filtered (0.45 μm) during collection, acidified with a drop of nitric acid (Suprapur, Sigma-Aldrich, Darmstadt, Germany) to preserve the fluid and avoid precipitation and absorption of elements onto the walls of the sample container. Anions were analyzed by ion chromatography (see Saby et al., 2022 for details). Most cations were analyzed at the Krafla laboratory by ICP-MS (details for the methods can be found in Hauksson and Gudmundsson, 2008). Strontium concentrations were determined by ICP-MS at the ALS laboratories, in Luleå, Sweden, and volatile metals were analyzed at McGill University, also by ICP-MS. The volatile metal ICP-MS analyses were conducted using a Thermo-Finnigan iCAP-Qc quadrupole MS with long dwell times per mass (100 msec) to achieve low detection limits. The instrument was calibrated against 5 dilutions of three volatile metal standards (two standards for Bi, Cd, Tl and Sb, and one for Hg, all at 1 ppt to 10 ppb). Dilutions were prepared by mass using nano-pure 2% HNO_3 as the diluting acid. Analyses were conducted in triplicate to determine precision.

Four units of fresh basalt were sampled across the þeistareykir area. Each unit was sampled at three different locations for a total of 12 samples. Altered rock cuttings collected at 1600 *m* depth in well þG-01 were provided by ÍSOR and are taken to represent the host rock for the geothermal reservoir. The samples consist of fragments of specifically chosen variably altered rock (from pristine magmatic fragments to chlorite-epidote-plagioclase-dominated altered fragments). The fragments were washed in de-ionized water, dried, and then divided into eight sub-samples to obtain a range in the degree of alteration. The fresh samples were crushed wrapped in Kraft paper using a steel hammer, dry coarse-milled in a WC ring mill, and wet fine-milled to less than 1 μm in a WC ball mill. The altered samples were crushed in an agate mortar and milled to below 1 μm by hand. The powder was then pressed into pellets (without additive) and analyzed by LA-ICP-MS at McGill University following the method of Garbe-Schönberg and Müller (2014). Further method details of the pellet analyses can be found in Saby et al. (2022).

5. Results

The fresh rocks have major and trace element compositions within the þeistareykir magmatic trend defined by literature data (extracted Jan-2022 from the GEOROC database - http://georoc.mpch-mainz.gwdg.de/georoc). Element concentrations in the altered rocks are higher than in the fresh rocks for most elements (Tables 1,2 and 3). Major oxide concentrations vary from 50.1 to 50.9 wt% for SiO_2, to 0.16 to 0.18 wt% for MnO, and Sr, V, Cr, Ni, Zn, and Zr are the most abundant

Table 3
Chemical composition of the altered rocks at the þeistareykir geothermal field.

Elements	þG-01-1600-s1	±	þG-01-1600-s2	±	þG-01-1600-s3	±	þG-01-1600-s4	±	þG-01-1600-s5	±	þG-01-1600-s6	±	þG-01-1600-s7	±	þG-01-1600-s8	±
wt%																
SiO2	50.87	4.54	50.42	4.52	50.71	4.53	50.10	4.50	50.10	4.50	50.37	4.51	50.40	4.51	50.69	4.53
TiO2	1.13	0.06	1.28	0.07	1.30	0.07	1.27	0.07	1.19	0.07	1.21	0.07	1.22	0.07	1.20	0.07
Al2O3	18.73	4.44	16.60	4.16	16.94	4.21	16.89	4.20	16.86	4.20	17.60	4.29	18.63	4.42	17.73	4.31
FeO	10.66	0.51	10.23	0.50	10.42	0.50	10.08	0.50	10.12	0.50	10.15	0.50	10.07	0.49	10.24	0.50
MnO	0.16	0.01	0.17	0.01	0.18	0.01	0.17	0.01	0.16	0.01	0.17	0.01	0.17	0.01	0.17	0.01
CaO	14.08	0.39	11.57	0.34	11.67	0.35	11.50	0.34	12.10	0.35	12.20	0.36	11.84	0.35	12.04	0.35
K2O	0.49	0.13	0.38	0.13	0.38	0.13	0.39	0.13	0.39	0.13	0.40	0.13	0.41	0.13	0.40	0.13
ppm																
Li	5.90	*n.d.*	6.70	*n.d.*	8.10	3.70	8.95	0.56	6.93	6.57	6.70	1.49	8.05	0.62	7.65	3.27
Na	18845.90	2.64	19927.60	3.04	17216.40	1.53	17280.55	0.90	19003.17	6.58	21031.75	6.39	21140.50	0.99	20519.15	4.58
K	2522.20	5.37	1616.85	0.53	1518.65	5.81	1571.90	0.28	1642.90	6.00	1623.10	6.57	1720.10	3.17	2385.25	1.11
Rb	5.35	0.93	3.50	14.29	3.40	2.94	3.30	3.03	3.83	1.30	3.60	2.78	3.65	1.37	4.80	12.50
Be	0.55	9.09	0.55	9.09	0.40	*n.d.*	0.30	*n.d.*	0.40	*n.d.*	0.60	*n.d.*	0.45	11.11	0.45	11.11
Mg	40515.70	3.23	48115.65	4.74	57918.20	3.76	59745.00	1.90	55593.57	5.15	50923.15	5.84	57286.60	0.77	56209.00	3.43
Sr	249.85	1.58	173.30	2.77	118.80	0.08	111.00	4.23	142.23	1.93	175.05	1.34	140.90	1.92	149.85	3.04
Ba	53.35	7.22	34.45	8.56	34.30	9.33	25.85	7.54	30.23	5.21	44.75	14.86	30.00	4.67	40.30	0.74
Ti	7703.45	0.68	8280.50	1.88	7754.00	0.10	7522.95	0.52	7243.93	5.75	8170.85	1.64	7544.50	1.55	7127.00	3.82
V	255.20	0.47	244.95	0.47	204.85	2.47	191.50	2.40	217.13	0.24	219.65	3.26	211.10	3.36	221.90	4.73
Cr	233.25	7.27	308.70	4.92	290.80	7.60	269.85	0.83	315.10	0.22	281.10	2.74	320.10	2.50	339.00	0.38
Mn	1541.20	3.52	1572.55	2.64	1612.25	2.68	1542.45	1.35	1533.27	2.57	1460.15	0.00	1586.75	1.41	1595.95	0.59
Fe	71459.45	0.95	65264.15	0.02	90099.40	2.95	93214.20	3.57	80913.83	4.88	74552.25	4.92	86558.80	5.43	81853.20	1.29
Co	57.55	1.48	64.00	2.66	87.40	3.78	88.00	0.45	76.60	1.99	68.35	4.75	84.30	6.41	80.40	0.25
Ni	63.90	1.25	75.15	1.93	107.95	2.18	113.15	2.17	92.97	5.90	82.65	5.63	105.15	8.32	105.55	0.52
Cu	27.50	5.82	50.60	1.58	18.00	3.89	14.80	15.54	36.90	16.10	16.30	8.59	22.05	15.19	18.70	2.67
Zn	92.60	2.59	101.60	2.17	128.15	2.77	124.50	1.20	112.20	0.53	103.95	7.07	118.30	6.59	116.65	3.04
Zr	127.40	3.77	146.30	6.43	104.75	1.77	96.00	3.33	102.47	3.91	129.40	*n.d.*	107.05	2.01	106.80	3.00
Nb	7.90	3.80	8.10	3.70	7.55	7.28	7.15	0.70	6.13	7.94	7.75	4.52	7.05	14.89	7.10	2.82
Mo	3.50	14.29	1.05	23.81	0.65	7.69	0.40	*n.d.*	0.60	*n.d.*	0.70	28.57	1.65	27.27	1.70	*n.d.*
Ag	*n.d.*		*n.d.*		*n.d.*		*n.d.*		*n.d.*		*n.d.*		*n.d.*		*n.d.*	
Cd	0.10	*n.d.*	0.05	100.00	0.05	100.00	*n.d.*		0.07	*n.d.*	0.05	100.00	0.10	*n.d.*	0.10	*n.d.*
Hf	3.80	5.26	4.65	3.23	3.40	2.94	2.80	3.57	3.33	1.45	4.00	7.50	3.10	6.45	3.30	3.03
Ta	0.45	11.11	0.50	*n.d.*	0.40	*n.d.*	0.40	*n.d.*	0.40	*n.d.*	0.50	*n.d.*	0.40	*n.d.*	0.35	14.29
W	0.90	33.33	0.20	*n.d.*	0.15	33.33	0.15	33.33	0.10	*n.d.*	0.10	*n.d.*	0.20	*n.d.*	0.20	*n.d.*
Al	91,473	1.64	88,895	1.77	80,652	1.20	80,873	2.60	84,961	4.46	85,233	1.12	83,244	0.99	83,944	4.08
Ga	20.35	3.19	16.75	3.28	17.75	3.10	18.00	1.11	16.93	0.29	17.05	6.16	18.00	3.33	18.30	2.73
In	0.10	*n.d.*	0.10	*n.d.*	0.05	100.00	*n.d.*		0.10	*n.d.*	0.10	*n.d.*	0.10	*n.d.*	0.10	*n.d.*
Sn	0.80	12.50	0.70	*n.d.*	0.55	9.09	0.60	*n.d.*	0.57	16.67	0.55	9.09	0.65	7.69	0.60	*n.d.*
Sb	0.10	*n.d.*	0.10	*n.d.*	0.10	*n.d.*	0.20	*n.d.*	0.10	*n.d.*	0.10	*n.d.*	0.20	*n.d.*	0.10	*n.d.*
Tl	*n.d.*		*n.d.*		*n.d.*		*n.d.*		*n.d.*		*n.d.*		*n.d.*		*n.d.*	
Pb	1.25	4.00	0.80	*n.d.*	0.75	6.67	0.65	7.69	0.73	6.67	1.15	4.35	0.85	5.88	0.80	*n.d.*
Bi	*n.d.*		*n.d.*		*n.d.*		*n.d.*		*n.d.*		*n.d.*		*n.d.*		*n.d.*	
Si	227,062	0.61	227,156	1.29	207,634	3.04	198,695	1.54	203,852	7.21	220,013	2.37	212,098	0.98	219,470	1.36
As	0.35	14.29	0.10	*n.d.*	0.10	*n.d.*	0.20	*n.d.*	0.13	33.33	0.10	*n.d.*	0.15	33.33	0.15	33.33
Se	0.15	100.00	0.25	20.00	0.10		0.10	*n.d.*	0.35	71.43	*n.d.*		0.30		0.05	
Sc	33.70	2.67	36.75	0.14	24.15	4.35	20.40	0.98	29.03	5.62	33.80	5.33	26.25	4.00	28.25	3.72
Y	29.60	6.42	32.45	4.47	21.15	3.55	19.50	0.51	21.93	2.21	27.50	1.45	21.65	5.77	22.55	4.66
La	7.95	6.92	7.00	8.57	6.95	5.04	6.20	*n.d.*	6.87	4.48	7.60	5.26	6.65	3.76	6.80	*n.d.*
Ce	14.85	9.09	13.85	9.03	16.20	12.35	16.35	10.70	14.60	9.85	14.95	2.34	16.05	1.56	15.20	2.63
Pr	2.40	8.33	2.45	2.04	2.45	6.12	2.35	10.64	2.23	2.44	2.40	4.17	2.35	6.38	2.40	*n.d.*
Nd	11.35	4.85	13.00	*n.d.*	11.80	5.08	11.15	4.04	11.17	1.42	12.50	3.20	11.50	7.83	11.60	3.45
Sm	4.10	*n.d.*	4.25	5.88	3.75	1.33	3.35	1.49	3.50	7.46	4.00	*n.d.*	3.60	8.33	3.60	2.78
Eu	1.40	7.14	1.45	10.34	1.20	*n.d.*	1.05	4.76	1.13	4.76	1.30	*n.d.*	1.20	*n.d.*	1.15	4.35

(*continued on next page*)

Table 3 (*continued*)

Elements	þG-01-1600-s1	±	þG-01-1600-s2	±	þG-01-1600-s3	±	þG-01-1600-s4	±	þG-01-1600-s5	±	þG-01-1600-s6	±	þG-01-1600-s7	±	þG-01-1600-s8	±
Gd	4.70	4.26	5.45	2.75	4.05	1.23	3.35	1.49	4.17	*n.d.*	4.70	8.51	3.95	1.27	3.95	3.80
Tb	1.10	*n.d.*	1.20	*n.d.*	0.90	*n.d.*	0.80	*n.d.*	0.90	5.88	1.00	10.00	0.80	*n.d.*	0.85	5.88
Dy	4.90	2.04	5.55	4.50	4.25	1.18	4.00	7.50	4.40	1.12	5.15	4.85	4.15	6.02	4.40	2.27
Ho	1.15	4.35	1.25	4.00	0.90	*n.d.*	0.80	*n.d.*	1.00	*n.d.*	1.10	*n.d.*	0.80	*n.d.*	0.95	5.26
Er	3.30	3.03	3.75	1.33	2.60	3.85	2.35	2.13	2.83	6.90	3.05	4.92	2.50	4.00	2.60	3.85
Tm	0.55	9.09	0.55	9.09	0.40	*n.d.*	0.40	*n.d.*	0.43	11.11	0.50	*n.d.*	0.40	*n.d.*	0.40	*n.d.*
Yb	3.05	4.92	3.40	2.94	2.45	2.04	2.30	*n.d.*	2.60	4.00	3.05	1.64	2.35	6.38	2.45	2.04
Lu	0.60	*n.d.*	0.65	7.69	0.40	*n.d.*	0.35	14.29	0.47	11.11	0.50	*n.d.*	0.40	*n.d.*	0.45	11.11
Th	0.60	*n.d.*	0.70	*n.d.*	0.50	*n.d.*	0.50	*n.d.*	0.50	*n.d.*	0.50	*n.d.*	0.45	11.11	0.50	*n.d.*
U	0.20	*n.d.*	0.10	*n.d.*	0.15	33.33	0.10	*n.d.*	0.10	*n.d.*	0.10	*n.d.*	0.10	*n.d.*	0.10	*n.d.*

trace elements. The altered samples show a linear trend extending from the magmatic trend defined for þeistareykir (Figs. 2 and 1A), representing a mixing curve between the precursor basalt and an entirely altered endmember. The elements presented in Fig. 2 are the ones who exhibit the best fits. It is unlikely that the alteration endmember is captured in the alteration dataset of the measured values, but the trend defines the direction of alteration. The precursor basalt is predicted to have a MgO content of 7 wt% and is close to the composition of samples þG-01-roc-09 and þG-01-roc-11, which are from the þeistareykjahraun lava flow. The altered rocks show up to 2.0–2.5 times enrichment in the immobile elements Zr, Nb, Hf, Th and U compared to the fresh basalt (Table 3), with this enrichment factor consistent among the elements. The LREE also give the same enrichment factor with the HREE somewhat lower (1.5–2.0). We interpret this to represent residual enrichment in these immobile elements during progressive alteration. The altered sample composition was therefore normalized to the precursor basalt content of these elements (following Grant, 2005), which allows for determining the release or sequestration of elements during alteration. This calculation shows leaching for all major elements except K, enrichment in Li, Cr and Sb, and leaching of the base metals, semi-volatile metals and the HREE + Sc (Fig. 3a and b). The elements with the most substantial relative change during alteration are Cu (leached) and Sb (enriched).

Fluid compositional data used in this study are reported in Table A1 and include $^{3}He/^{4}He$ ratios, major elements, and trace volatile metals. Additional data for these samples has previously been reported in Saby et al. (2022). The $^{3}He/^{4}He$ ratios are reported uncorrected for the atmospheric component (R/Ra) and corrected for this component (Rc/Ra) using the $^{4}He/^{20}Ne$ ratio as an index of the atmospheric helium contribution (following Torgersen and Jenkins, 1982):

$$Rc \,/\, Ra = \left[(R/Ra)_{meas} - r\right] / (1 - r) \tag{1}$$

$$r = \left(^{4}He/^{20}Ne\right)_{ASW} \Big/ \left(^{4}He/^{20}Ne\right)_{meas} \tag{2}$$

where $(R/Ra)_{meas}$ is the measured helium isotopic ratio, and $(^{4}He/^{20}Ne)_{ASW}$ and $(^{4}He/^{20}Ne)_{meas}$ are the ratio calculated at solubility equilibrium with water (or ASW) at 3.7 °C (mean annual atmospheric temperature or MAAT) and the measured ratio in sample, respectively.

Metal concentration in fluids sampled at the wellhead is low, as is the case for most geothermal fields in Iceland (Ármannsson, 2015). The volatile metals show values ranging from Hg 0.066–0.192 ppb, Bi 0.012–0.042 ppb, Cd 0.024–0.029 ppb, Tl 0.038–0.089 ppb, As 0.41–230 ppb and Sb 0.005–1.2 ppb (Table 1).

6. Discussion

6.1. Water-rock interaction and magma degassing contributions to deep geothermal fluids

The composition of the deep reservoir fluids has been determined for þeistareykir by direct down-well sampling (Saby et al., in 2022). This study showed that the deep fluids are relatively enriched in base metals and (semi) volatile metals (in particular Te, Hg, Re, and Tl) compared to local basalt, interpreted as element input from both magma degassing and water-rock interaction. To verify and quantify the contributions from these two sources, knowledge of their respective elemental signature is required.

The element signature of the fluid released by magma degassing can be estimated from the enrichment factors and the composition of the þeistareykir tholeiitic basalt. Here, we use the element enrichment factors as determined for Kilauea basalt (Mather et al., 2012) and calculate an estimate of the emitted fluid composition for an element *i* using the equation:

$$C_i^{fluid} = EF_i * C_i^{\text{þG-basalt}} \tag{3}$$

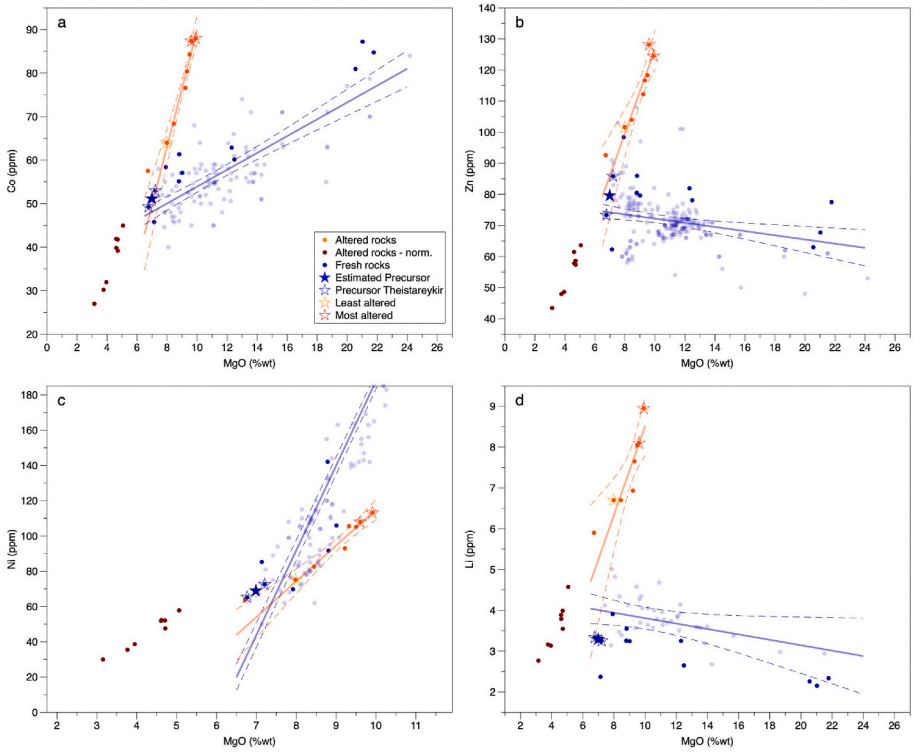

Fig. 2. Alteration trends of variably altered rocks and fresh rocks at þeistareykir for Co (a), Zn (b), Ni (c), Li (d) against MgO, as examples. All the plots can be found in Fig. A1, in the supplementary material. The light blue dots represent the þeistareykir magmatic trend defined by literature data (extracted Jan-2022 from the GEOROC database - http://georoc.mpch-mainz.gwdg.de/georoc). The dotted lines represent the confidence interval of the trend at 95%. The altered rocks have been specifically sampled in different alteration states to evaluate the trends.

Where C is the concentration of element *i* in the respective phase and EF the enrichment factor for that element. These enrichment factors for Kilauea represent surface volatility. In contrast, the magma degassing at þeistareykir occurs at elevated pressure in the subsurface, and pressure impacts the volatility of the elements (e.g. Migdisov et al., 2014). However, enrichment factors at elevated pressure are only available for a small subset of elements, which limits the ability to differentiate between magma degassing and water-rock interaction. Therefore, we use the EF data at atmospheric pressure, assuming that the resulting chemical fingerprint is not overly affected by pressure, although absolute values will be.

To scale the resulting composition to the concentration range found in the deep fluid sample, we assume all Cl in the fluid is derived from magma degassing. The Cl content of the unaltered rocks is low (*ca.* 60 mg/kg, GEOROC) and is generally higher for the altered equivalents, so Cl release from water-rock interaction can be expected to be negligible. There is also no evidence of a seawater contribution to þeistareykir geothermal fluids (Saby et al., 2020; Pinti et al., 2022). Direct Cl magma degassing is unlikely to be significant at þeistareykir given the low Cl abundance in the basalt and the late degassing of Cl (cf. Witham et al., 2012). Yet, partition coefficients indicate that Cl would partition into the exsolving water-rich fluid (D fluid-melt >10 for Etna basalt – Alletti et al., 2009) and hence be strongly mobilized in magma degassing.

To calculate the mass transfer in water-rock interaction, we use the difference between the immobile-element corrected altered rock composition and that of the precursor basalt and scale this elemental signature by assuming that Na is exclusively derived from WRI. Sodium was chosen as it has a low EF (1.7), strong release in water rock interaction (40% change in composition) and we have precise Na data for all samples. The scaling only shifts the concentration up or down and does not change the elemental signature. The resulting compositional signatures are shown in Fig. 4, together with the measured concentrations in the þeistareykir fluid sampled at 1600 *m* depth.

Fig. 4 shows a remarkable agreement between the estimated fluid derived from magma degassing and the measured composition of deep þeistareykir geothermal fluid. The elemental patterns trace each other, and even the absolute concentrations are within an order of magnitude for most elements. In contrast, the WRI elemental signature is distinctly different (Fig. 4). This suggests that the deep fluid composition is predominantly controlled by magmatic input rather than by water-rock interaction. The only elements that deviate significantly are the alkalis and the base metals, particularly copper (Cu). Water-rock interaction acts as a sink of Li and K and can, therefore, not explain the alkali concentrations. However, the leaching of base metals that accompanies WRI can explain these concentrations in the deep fluid. Moreover, WRI can explain the higher concentrations of V and Ti and lower concentrations of Cr, Zr, Nb, and Hf, with the former two being leached and the latter four being sequestered in WRI.

The base and refractory metals, for which both magma degassing and rock leaching contribute to the fluid composition, can be used to estimate a mean magmatic degassing contribution of 80%, with the remaining 20% derived from water-rock interaction. Among the base metals, Cu is most prominently leached in WRI, giving values of 77% sourced from degassing and 23% for WRI. Applying the same approach to a deep fluid sample collected in the adjacent Krafla geothermal field gives similar results, with a mean magmatic contribution of 82% and 18% from WRI. For this well, the magmatic signature calculation is based on fresh Krafla basalt element concentrations and the above-mentioned enrichment factors (eqn. (3)), but the WRI signature is taken from þeistareykir data because of data on alteration in Krafla well K-21. Despite the more significant uncertainty in the Krafla results because of the unknown WRI signature for Krafla, it is clear that for both geothermal fields, the dominant source of elements is fluid released from the magma, except for Mn, Fe, Co, Cu, Ti and V.

The magmas erupted at þeistareykir show a negligible crustal contribution and minimal fractional crystallization and are considered

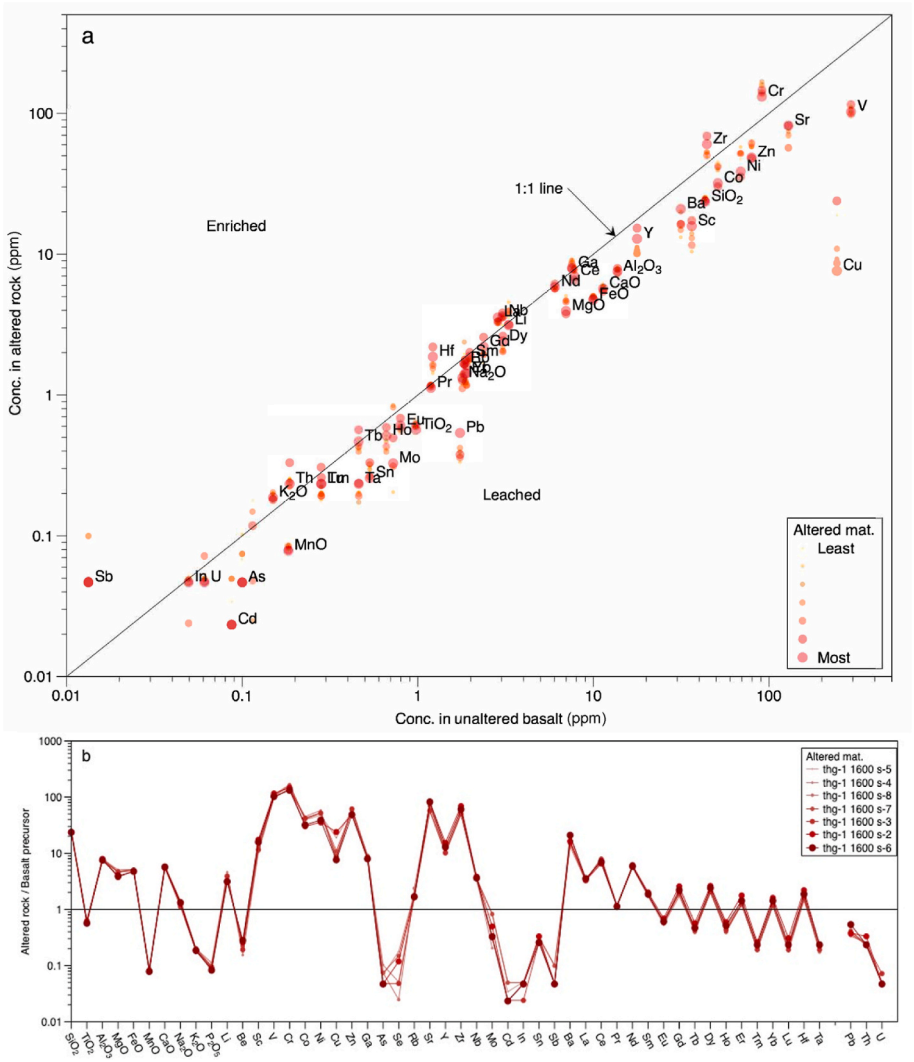

Fig. 3. Comparison of the concentrations of elements between altered rock and fresh basalt. a. Concentration in ppm of 8 sub-samples of variably altered rocks against the average concentration in fresh rocks. b. Variably altered rocks normalized to the fresh rocks.

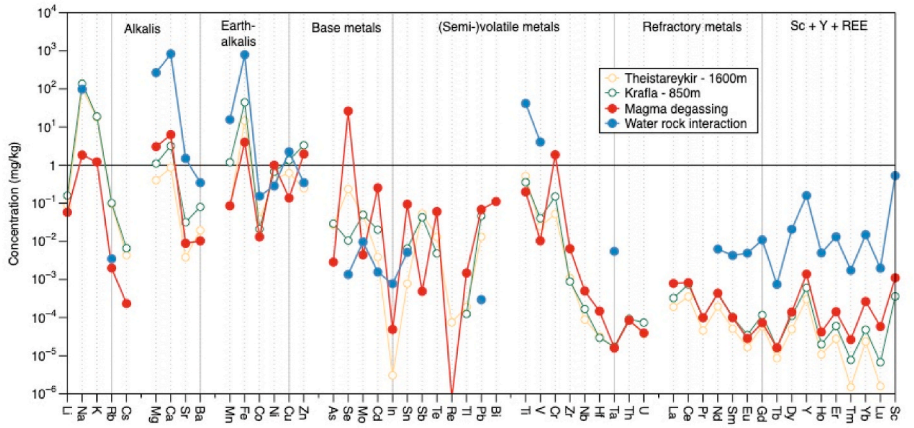

Fig. 4. Estimation of the magmatic and water-rock interaction contributions using the enrichment factors (EF) for every element. All the details can be found in Saby et al. (2022).

close in composition to primary partial melts from the mantle (Eiler, 2000; Stracke et al., 2003; Mutch et al., 2019). Therefore, the metals these magmas contribute to the geothermal fluids in magmatic degassing are therefore mantle-derived and represent a primary fertilization of the crust. Such a transfer from the mantle is well established for the noble gases (e.g. Ozima and Zahnle, 1993). Recently, it has been proposed that metals could be added to the deep crust via sulfides (e.g. Locmelis et al., 2016), but in this case, it takes place in the shallow crust.

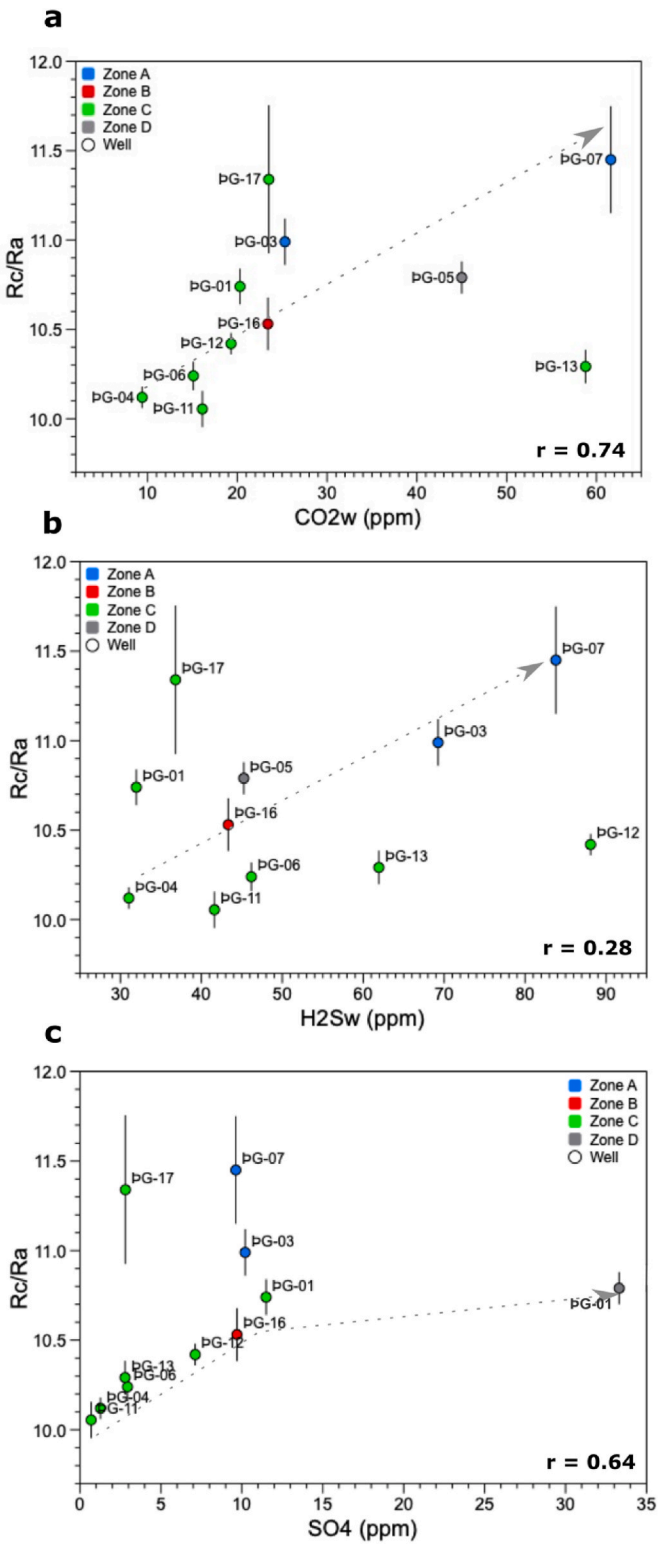

Fig. 5. The Rc/Ra ratio compared to the major gases CO_2 (a) and H_2S (b), and to SO_4 (c). The trends shown are visual fits to the data. The r value corresponds to the Spearman's correlation coefficient.

Moreover, whereas deep fertilization mainly involves chalcophile elements (see Locmelis et al., 2016), at þeistareykir mantle-to-crust transfer is heavily biased to the (semi) volatile metals (Saby et al., 2022).

6.2. Magma degassing constrained using noble gases

The deep fluid composition in þeistareykir is only known from one well (þG-01). Therefore, it is impossible to assess any variations in the spatial contributions from magma degassing and WRI throughout the field. However, fluids sampled at the wellhead are available for the entire field. Noble gases are a robust tool to estimate the contribution of volatiles in geothermal fluids sourced from the mantle (M), the crust (C) and the atmosphere (A – via meteoric recharge). Here, we calculate the percentage contribution for each source from the helium isotopes using ternary mixing equations (Pinti et al., 2019):

$$R/Ra_{observed} = R/Ra_{mantle}*M + R/Ra_{crust}*C + R/Ra_{ASW}*A \quad (4)$$

$$1/(^4He/^{20}Ne)_{observed} = M/(^4He/^{20}Ne)_{mantle} + C/(^4He/^{20}Ne)_{crust} + A/(^4He/^{20}Ne)_{ASW} \quad (5)$$

$$M + C + A = 1 \quad (6)$$

Where the subscripts observed, mantle, crust, and ASW, refer to the observed sample, the mantle end-member (R/Ra = 11.45 and $^4He/^{20}Ne$ = 1000; Sano and Wakita, 1985; Saby et al., 2020), the crustal end-member (R/Ra = 0.02 and $^4He/^{20}Ne$ = 1000; Sano and Wakita, 1985), and the meteoric water end-member (R/Ra = 1 and $^4He/^{20}Ne$ = 0.251 calculated at ASW conditions of 3.7 °C, the average recharge temperature of the field, respectively, and M, C, and A are the fractions of the mantle, crust, and atmospheric components. For well þG-11 (which exhibits the lowest measured R/Ra value) with $^4He/^{20}Ne$ = 29.77 and an R/Ra = 9.96 (Table A1), the percentage of helium derived from mantle in the mixture is 87.0 %, compared with 12.2 % of crustal helium and 0.82 % of atmospheric helium. Well þG-01 gives 93.5%, 6.2% and 0.3%, and for the well with the highest R/Ra value, þG-07, the relative contributions are 89.1%, 10.8% and 0.1%. These results are consistent with the previously calculated 80% contribution of magmatic degassing based on the metals in the deep fluid sample, and support a strong magmatic contribution to the fluids, both in noble gases and in metals. The magmatic contribution is higher for the noble gases, which likely reflects their higher volatility than metals and, therefore, their preferential release from the magma (Paonita, 2005). These results thus indicate a clear and direct transfer of volatiles and metals from the magma to the geothermal fluid reservoir.

The contributions of mantle, crust, and atmosphere across the geothermal field indicate that the wells with the highest mantle contributions are the ones closest to the Bæjarfjall and Ketilfjall mountains (Fig. 1). This suggests the impact of local and regional structures and faults on the fluid pathway from depth to surface (see Khodayar et al., 2018). These highest contributions are in the field areas with the highest major gas species abundances (Khodayar et al., 2018).

These results indicate that the $^3He/^4He$ ratio can be used at the scale of the field as a measure of the relative magma degassing contribution, which, when combined with the metal concentrations in the fluids can then reveal the relative importance of magma and the leaching of rocks by hot fluids to the content of a given metal. A dominant magmatic contribution of metals would be associated with relatively high $^3He/^4He$ ratios owing to input of primordial ^3He, while water-rock interaction would favor the release of radiogenic ^4He produced by the decay of U and Th contained in the reservoir rocks, and thus have a lower $^3He/^4He$ ratio. We also make the explicit assumption that the magmatic signature of helium is homogeneous at the scale of the field, and thus, any variation in the $^3He/^4He$ in the field is only related to a radiogenic contribution of ^4He. The Rc/Ra ratio shows strong positive correlations with the major magmatic gases (CO_2, H_2S) and SO_4 (Fig. 5a, b, c), which further supports that this represents the magmatic contribution.

Fig. 6 presents the Rc/Ra ratio of the þeistareykir well vapor phase sampled at the wellhead against the Cl-normalized metal content in the corresponding surface fluids, focusing on the most volatile metals. We normalize to Cl here to remove the effect of any shallow dilution,

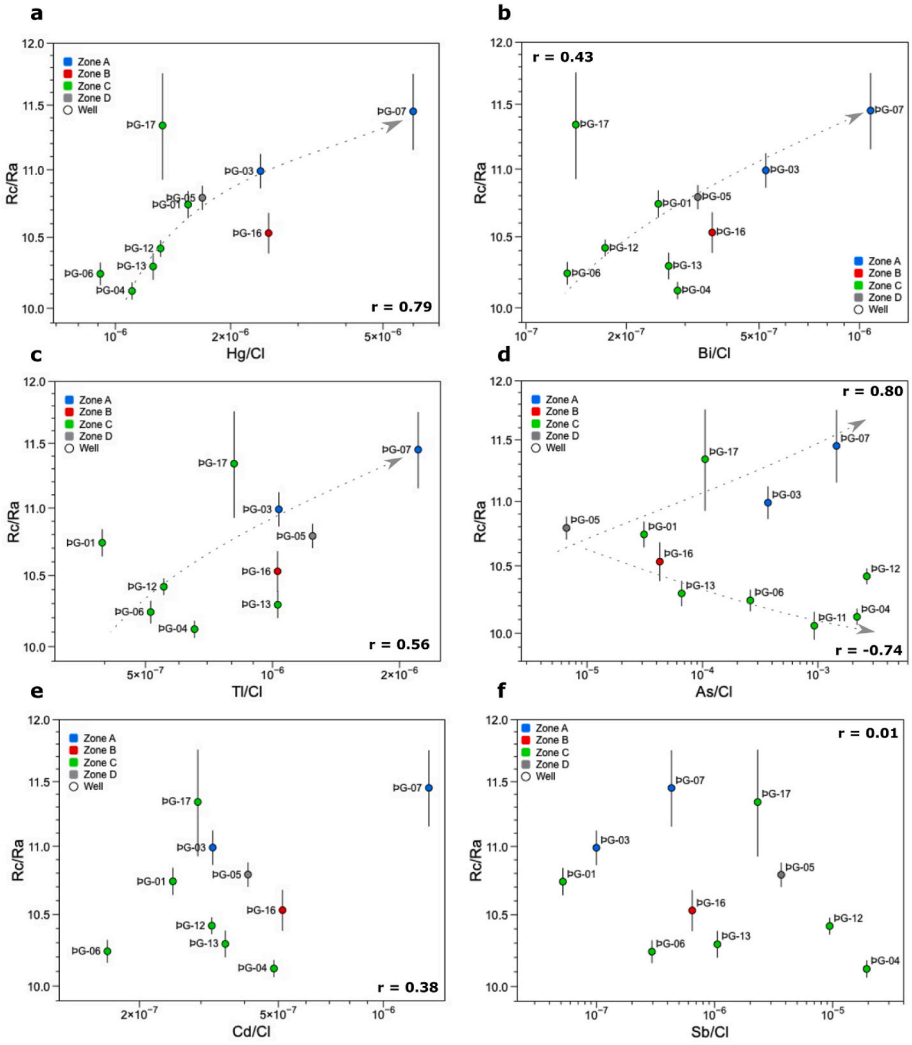

Fig. 6. The Rc/Ra ratio compared to the most volatile metals (Hg (a), Bi (b), Tl (c), Cd (d), As (e) and Sb (f)) normalized to chlorine. The trends shown are visual fits to the data. The r value corresponds to the Spearman's correlation coefficient.

assuming conservative behavior of Cl. Results show that Hg and Bi, which are among the most volatile of the metals (e.g., Mather et al., 2012) have a well-defined positive correlation with the Rc/Ra ratio, with potentially a subtle WRI contribution in Bi for wells þG-04, þG-13 and þG-16. This clear positive correlation suggests that Hg and Bi can be used as a tracer of magma degassing. The behavior of Cd, Tl and As is more complex. Wells þG-01, þG-03, þG-05, þG-17 and þG-07 show a positive correlation with Rc/Ra, whereas þG-04, þG-06, þG-12, þG-13 and þG-16 display a negative correlation. This suggests sourcing from both magma degassing and WRI, with the relative importance of each source varying among the wells and hence spatially in the geothermal field. The wells that present the highest magmatic contribution for the metals evaluated here are wells þG-07, þG-03, þG-05, þG-01 and þG-17.

The metal/Cl ratios also correlate with the major gas species (CO_2, H_2S) and with SO_4 content of the fluid (Fig. 7). This reflects derivation of the same source, i.e. magma degassing, but may also contain a component related to stronger solvation at higher ligand content.

The metal/Cl data trends show a larger scatter than in volatiles (Figs. 6 and 7). This may partly reflect the more significant analytical uncertainty in the metal data. In addition, the surface fluids represent the vapor fraction following boiling of the geothermal reservoir fluid, and as shown in Saby et al. (2022), are strongly depleted in most elements compared to the deep fluid. Transfer of the deep elemental signature to the surface is thus highly sensitive to boiling. Boiling also complicates the use of surface fluids sampled at the well head in determining the absolute contributions of the two metal sources for metals that are less volatile, that create strong complexes with ligands, and that prefer the residual fluid phase. Boiling can affect noble gas elemental ratios but not the isotopic ones, so the pristine Rc/Ra ratio of the source is preserved.

7. Conclusions

This study of noble gases and volatile metals in geothermal fluids was carried out to establish the respective contributions of magma degassing and water-rock interaction to the metal content of basalt-hosted magmatic-hydrothermal fluids, and to determine the variability in these contributions across the þeistareykir geothermal field in north-eastern Iceland. The estimated magma degassing elemental signature, combined with the measured water-rock interaction mass transfer indicates that the metal load of the deep geothermal reservoir fluid is dominated by magma degassing input, except for Mn, Fe, Co, Cu, V and Ti. Helium isotopic data for well-head fluids confirm this, both data sources suggesting an approximately 80–85% contribution from magma and 15–20% from water-rock interaction. Geothermal fluid samples from production wells show atmosphere-normalized $^3He/^4He$ ratios (Rc/Ra) from 9.44 to 11.45 which are interpreted to represent mixing between a fluid carrying a pure magmatic ^{3}He-enriched component and

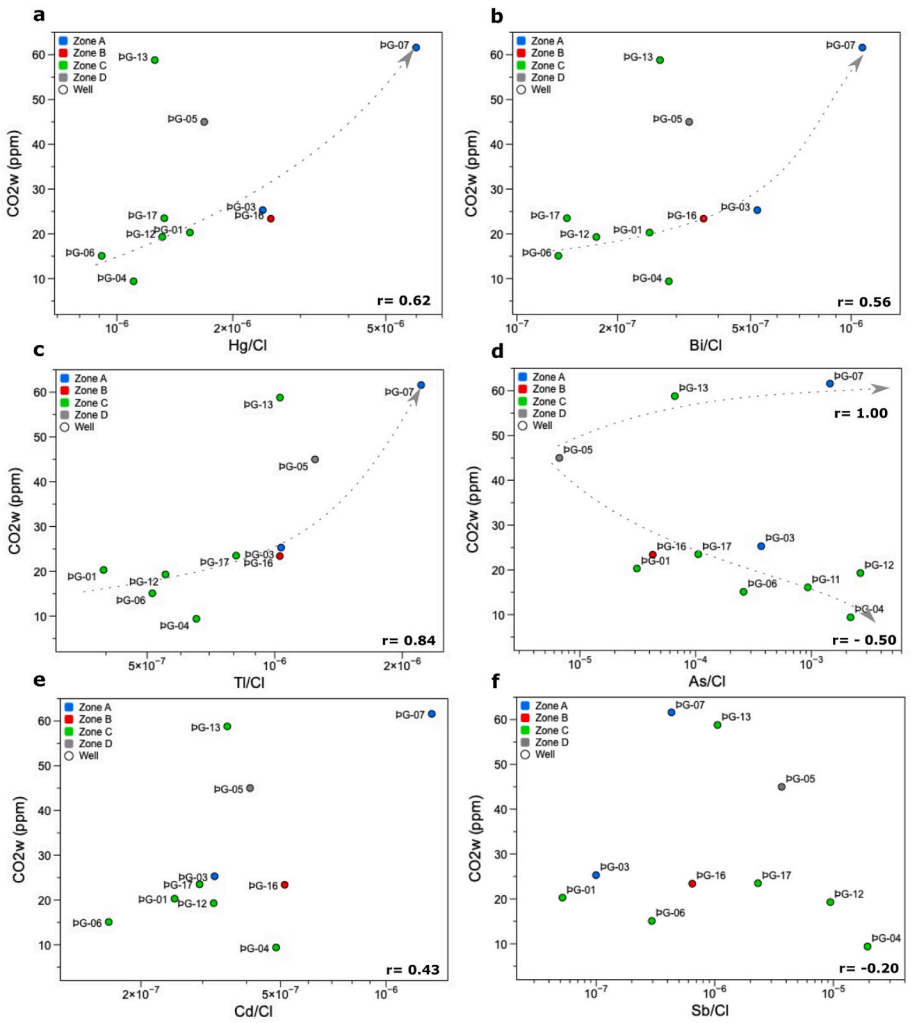

Fig. 7. Volatile metals (Hg (a), Bi (b), Tl (c), Cd (d), As (e) and Sb (f)) normalized to chlorine compared to the major gas CO_2. The trends shown are visual fits to the data. The r value corresponds to the Spearman's correlation coefficient.

a crustal component with helium slightly diluted by radiogenic ^{4}He. The latter is considered a measure of water-rock interaction. The Rc/Ra values show variability in field magma degassing and WRI contributions. Volatile metals correlate with Rc/Ra and similarly vary across the field, with Hg and Bi the best indicators of the magmatic contribution. Noble gases and volatile metals thus provide tools to identify and quantify the relative contributions of magma degassing and water-rock interaction to the metal load of geothermal fluids and to track how these vary in space and time.

CRediT authorship contribution statement

Marion Saby: Writing – original draft, Methodology, Investigation, Funding acquisition, Formal analysis, Data curation, Conceptualization. **Vincent van Hinsberg:** Writing – review & editing, Validation, Supervision, Resources, Project administration, Funding acquisition, Conceptualization. **Daniele L. Pinti:** Writing – review & editing, Validation, Supervision, Resources, Project administration, Methodology, Funding acquisition, Data curation, Conceptualization. **Kim Berlo:** Writing – review & editing, Resources. **Bjarni Gautason:** Writing – review & editing, Supervision, Resources, Project administration, Funding acquisition, Conceptualization. **Ásgerður Sigurðardóttir:** Writing – review & editing, Supervision, Resources, Project administration, Funding acquisition, Data curation. **M. Clara Castro:** Writing – review & editing, Formal analysis.

Declaration of competing interest

The authors declare that they have no known competing financial interests or personal relationships that could have appeared to influence the work reported in this paper.

Acknowledgements

We warmly thank André Poirier and Julien Gogot for their help with sample preparation, analyses, and preparation of sampling material prior to field work. This research was funded by the Natural Sciences and Engineering Research Council of Canada (NSERC) through an Alexander-Graham-Bell-doctorate (BESC D) grant (CGSD3-503679-2017) to M.S., Discovery Grants to D.L.P. (RGPIN-2015-05378) and Discovery Grants to V.V.H. and K.B. (RGPIN-2014-03882); by the Fonds de recherche du Québec - Nature et technologies (FRQNT - Grant 2018-RS-203300) through Geotop's Collaborative Projects Program (grants GEOTOP-03-2018 and GEOTOP-10-2020); by ÍSOR and the Landsvirkjun Power company; and by Osisko philantrophy. We also thank ÍSOR, Landsvirkjun, and the University of Iceland for providing access to sampling locations and to their facilities.

Appendix A. Supplementary data

Supplementary data to this article can be found online at https://doi.

org/10.1016/j.apgeochem.2024.106213.

Data availability

Data will be made available on request.

References

Aiuppa, A., Baker, D.R., Webster, J.D., 2009. Halogens in volcanic systems. Chem. Geol. 263, 1–18.

Allègre, C.J., Moreira, M., Staudacher, T., 1995. $^{4}He/^{3}He$ dispersion and mantle convection. Geophys. Res. Lett. 22 (17), 2325–2328.

Alletti, M., Baker, D.R., Scaillet, B., Aiuppa, A., Moretti, R., Ottolini, L., 2009. Chlorine partitioning between a basaltic melt and H2O–CO2 fluids at Mount Etna. Chem. Geol. 263 (1–4), 37–50.

Ármannsson, H., 2015. The fluid geochemistry of Icelandic high temperature geothermal areas. Appl. Geochem. 66, 14–64.

Ármannsson, H., Gíslason, G., Torfason, H., 1986. Surface exploration of the Theistareykir high-temperature geothermal area, Iceland, with special reference to the application of geochemical methods. Appl. Geochem. 1, 47–64.

Ballentine, C.J., Burnard, P.G., 2002. Production, release and transport of noble gases in the continental crust. Rev. Mineral. Geochem. 47, 481–538.

Barnes, H., Seward, T., 1997. Geothermal systems and mercury deposits. Geochemistry of hydrothermal ore deposits 3, 699–736.

Berger, B.R., Bethke, P.M., 1985. Geology and Geochemistry of Epithermal Systems. Society of economic geologists.

Birkle, P., Portugal Marín, E., Pinti, D.L., Castro, M.C., 2016. Origin and evolution of geothermal fluids from Las Tres Vírgenes and Cerro Prieto fields, Mexico - Co-genetic volcanic activity and paleoclimatic constraints. Appl. Geochem. 65, 36–53.

Bodnar, R.J., 1995. Fluid inclusion evidence for a magmatic source for metals in porphyry copper deposits. In: Thompson, J.F.H. (Ed.), Magmas, Fluids and Ore Deposits, vol. 23. Mineralogical Association of Canada Short Course Series, pp. 139–152.

Breddam, K., Kurz, M.D., 2001. Helium isotope signatures of Icelandic alkaline lavas. EOS Trans Am Geophys Union. 82, F1315.

Breddam, K., Kurz, M.D., Storey, M., 2000. Mapping out the conduit of the Iceland mantle plume with helium isotopes. Earth Planet Sci. Lett. 176, 45–55.

Burnard, P.G., Polya, D.A., 2004. Importance of mantle derived fluids during granite associated hydrothermal circulation: He and Ar isotopes of ore minerals from Panasqueira 1 1 Associate editor: R. Wieler. Geochim. Cosmochim. Acta. 68 (7), 1607–1615.

Burnard, P.G., Hu, R., Turner, G., Bi, X.W., 1999. Mantle, crustal and atmospheric noble gases in Ailaoshan Gold deposits, Yunnan Province, China. Geochim. Cosmochim. Acta. 63 (10), 1595–1604.

Burnard, P., Graham, D., Farley, K., 2004. Fractionation of noble gases (He, Ar) during MORB mantle melting: a case study on the Southeast Indian Ridge. Earth Planet Sci. Lett. 227 (3), 457–472.

Carroll, M.R., Draper, D.S., 1994. Noble gases as trace elements in magmatic processes. Chem. Geol. 117, 37–56.

Chambefort, I., Stefansson, A., 2020. Fluids in geothermal systems. Elements 16, 407–411.

Christenson, B., Wood, C., 1993. Evolution of a vent-hosted hydrothermal system beneath ruapehu crater lake, New Zealand. Bull. Volcanol. 55 (8), 547–565.

Clark, J.R., Williams-Jones, A.E., 1990. Analogues of epithermal gold–silver deposition in geothermal well scales. Nature 346 (6285), 644–645.

Clarke, W.B., Jenkins, W.J., Top, Z., 1976. Determination of tritium by mass spectrometric measurement of ^{3}He. Int. J. Appl. Radiat. Isot. 27, 515–522.

Crowe, B.M., Finnegan, D.L., Zoller, W.H., Boynton, W.V., 1987. Trace element geochemistry of volcanic gases and particles from 1983–1984 eruption episodes of Kilauea volcano. J. Geophys. Res. 92 (13), 714, 708–13.

Darling, G., Ármannsson, H., 1989. Stable isotope aspects of fluid flow in the Krafla, Námafjall and Theistareykir geothermal systems of northeast Iceland. Chem. Geol. 76, 197–213.

Edmonds, M., Mather, T.A., Liu, E.J., 2018. A distinct metal fingerprint in arc volcanic emissions. Nat. Geosci. 11, 790–794.

Eiler, J.M., 2000. Oxygen isotope geochemistry of oceanic-arc lavas. J. Petrol. 41 (2), 229–256. https://doi.org/10.1093/petrology/41.2.229.

Füri, E., Hilton, D.R., Halldórsson, S.A., Barry, P.H., Hahm, D., Fischer, T.P., Grönvold, K., 2010. Apparent decoupling of the He and Ne isotope systematics of the Icelandic mantle: the role of He depletion, melt mixing, degassing fractionation and air interaction. Geochim. Cosmochim. Acta. 74, 3307–3332.

Gamo, T., Okamura, K., Charlou, J.-L., Urabe, T., Auzende, J.-M., Ishibashi, J., Shitashima, K., Chiba, H., 1997. Acidic and sulfate-rich hydrothermal fluids from the Manus back-arc basin, Papua New Guinea. Geology. 25 (2), 139–142.

Gamo, T., Ishibashi, J., Tsunogai, U., Okamura, K., Chiba, H., 2006. Unique geochemistry of submarine hydrothermal fluids from arc-back-arc settings of the western pacific. Back-Arc spreading systems: geological, biological, chemical, and physical interactions. Geophys. Monogr. 166, 147–161.

Gena, K., Mizuta, T., Ishiyama, D., Urabe, T., 2001. Acid-sulphate type alteration and mineralization in the Desmos caldera, manus back-arc basin, Papua New Guinea. Resour. Geol. 51 (1), 31–44.

Giggenbach, W., 1992. Isotopic shifts in waters from geothermal and volcanic systems along convergent plate boundaries and their origin. Earth Planet Sci. Lett. 113, 495–510.

Gundfinnsson, G.H., 2014. Alteration in the Theistareykir geothermal system. A study of drill cuttings in thin sections. LV report.: LV-2014-063. 110.

Hauksson, T., Gudmundsson, 2008. Krafla. Acid Wells. Landsvirkjun, Report, p. 17.

Hedenquist, J.W., Henley, R.W., 1985. Hydrothermal eruptions in the Waiotapu geothermal system, New Zealand; their origin, associated breccias, and relation to precious metal mineralization. Econ. Geol. 80 (6), 1640–1668.

Hedenquist, J.W., Lowenstern, J.B., 1994. The role of magmas in the formation of hydrothermal ore deposits. Nature 370 (6490), 519–527.

Hedenquist, J.W., Simmons, S.F., Giggenbach, W.F., Eldridge, C.S., 1993. White Island, New Zealand, volcanic-hydrothermal system represents the geochemical environment of high-sulfidation Cu and Au ore deposition. Geology. 21 (8), 731–734.

Hedenquist, J.W., Arribas, A., Reynolds, T.J., 1998. Evolution of an intrusion-centered hydrothermal system; Far Southeast-Lepanto porphyry and epithermal Cu-Au deposits, Philippines. Econ. Geol. 93 (4), 373–404.

Hedenquist, J.W., Taguchi, S., Shinohara, H., 2018. Features of large magmatic–hydrothermal systems in Japan: characteristics similar to the tops of porphyry copper deposits. Resour. Geol. 68 (2), 164–180.

Henley, R.W., Barton, P., Truesdell, A., Whitney, J., 1984. Fluid-mineral Equilibria in Hydrothermal Systems, vol. 1. Society of Economic Geologists El, Paso, TX.

Hermannsson, S., Líndal, B., 1951. Chemical analysis of warm and hot springs. State Drilling Company, Jarðboranir Ríkisins, p. 32 (in Icelandic).

Hilton, D.R., Grönvold, K., O'Nions, R.K., Oxburgh, E.R., 1990. Regional distribution of ^{3}He anomalies in the Icelandic crust. Chem. Geol. 88, 53–67.

Hinkley, T.K., 1991. Distribution of metals between particulate and gaseous forms in a volcanic plume. Bull. Volcanol. 53, 395–400.

Hu, R., Burnard, P., Turner, G., Bi, X., 1998. Helium and argon isotope systematics in fluid inclusions of Machangqing copper deposit in west Yunnan Province, China. Chem. Geol. 146 (1), 55–63.

Kendrick, M.A., Duncan, R., Phillips, D., 2006. Noble gas and halogen constraints on mineralizing fluids of metamorphic versus surficial origin: Mt Isa, Australia. Chem. Geol. 235, 325–351.

Khodayar, M., Björnsson, S., Kristinsson, S.G., Karlsdóttir, R., Ólafsson, M., Víkingsson, S., 2018. Tectonic control of the Theistareykir geothermal field by rift and transform zones in North Iceland: a multi-disciplinary approach. Open J. Geol. 8, 543–584.

Kristinsson, S.G., Fridriksson, Th, Ólafsson, M., Gunnarsdóttir, S.H., Níelsson, S., 2013. The Theistareykir, Krafla and Námafjall high-temperature geothermal areas. Monitoring of surface activity and groundwater. Iceland GeoSurvey, report ÍSOR-2013/037. 152 (in Icelandic).

Krupp, R.E., Seward, T.M., 1987. The Rotokawa geothermal system, New Zealand; an active epithermal gold-depositing environment. Econ. Geol. 82 (5), 1109–1129.

Krupp, R.E., Seward, T.M., 1990. Transport and deposition of metals in the Rotokawa geothermal system, New Zealand. Miner. Deposita 25 (1), 73–81.

Landis, G.P., Rye, R.O., 2005. Characterization of gas chemistry and noble-gas isotope ratios of inclusion fluids in magmatic-hydrothermal and magmatic-steam alunite. Chem. Geol. 215 (1–4), 155–184.

Libbey, R., Williams-Jones, A., 2016. Lithogeochemical approaches in geothermal system characterization: an application to the Reykjanes geothermal field, Iceland. Geothermics 64, 61–80.

Locmelis, M., Fiorentini, M.L., Rushmer, T., Arevalo, R., Adam, J., Denyszyn, S.W., 2016. Sulfur and metal fertilization of the lower continental crust. Lithos 244, 74–93. https://doi.org/10.1016/j.lithos.2015.11.028.

Lowenstern, J.B., van Hinsberg, V., Berlo, K., Liesegang, M., Iacovino, K., Bindeman, I.N., Wright, H.M., 2018. Opal-A in glassy pumice, acid alteration, and the 1817 phreatomagmatic eruption at kawah ijen (java), Indonesia. Front. Earth Sci. 6, 11.

MacLennan, J., Jull, M., McKenzie, D., Slater, L., Grönvold, K., 2002. The link between volcanism and deglaciation in Iceland. G-cubed. 3, 1062.

Mamyrin, B.A., Tolstikhin, I.N., 1984. Helium Isotopes in Nature. Elsevier, Amsterdam.

Manning, A.H., Hofstra, A.H., 2017. Noble gas data from Goldfield and Tonopah epithermal Au-Ag deposits, ancestral Cascades Arc, USA: evidence for a primitive mantle volatile source. Ore Geol. Rev. 89, 683–700.

Mather, T.A., Witt, M.L.I., Pyle, D.M., Quayle, B.M., Aiuppa, A., Bagnato, E., et al., 2012. Halogens and trace metal emissions from the ongoing 2008 summit eruption of Kılauea volcano, Hawaii. Geochem. Cosmochim. Acta 83 (C), 292–323.

Mazor, E., Truesdell, A., 1984. Dynamics of a geothermal field traced by noble gases: cerro Prieto, Mexico. Geothermics 13 (1), 91–102.

Migdisov, A.A., Bychkov, A.Y., Williams-Jones, A.E., van Hinsberg, V.J., 2014. A predictive model for the transport of copper by HCl-bearing water vapour in ore-forming magmatic-hydrothermal systems: implications for copper porphyry ore formation. Geochem. Cosmochim. Acta 129, 33–53.

Moune, S., Sigmarsson, O., Thordarson, T., Gauthier, P.-J., 2006. Recent volatile evolution in the magmatic system of Hekla volcano, Iceland. Earth Planet Sci. Lett. 255 (3–4), 373–389.

Mutch, E.J.F., Maclennan, J., Shorttle, O., Edmonds, M., Rudge, J.F., 2019. Rapid transcrustal magma movement under Iceland. Nat. Geosci. 12 (7), 569–574. https://doi.org/10.1038/s41561-019-0376-9.

Nadeau, O., Stix, J., Williams-Jones, A.E., 2016. Links between arc volcanoes and porphyry-epithermal ore deposits. Geology. 44 (1), 11–14.

Norton, D.L., 1984. Theory of hydrothermal systems. Annu. Rev. Earth Planet Sci. 12, 155–177.

Óskarsson, F., Ármannsson, H., Ólafsson, M., Sveinbjörnsdóttir, Á.E., Markússon, S.H., 2013. The Theistareykir geothermal field, NE Iceland: fluid chemistry and production properties. Proc. Earth Planet. Sci. 7, 644–647.

Ozima, M., Zahnle, K., 1993. Mantle degassing and atmospheric evolution: noble gas view. Geochem. J. 27 (4/5), 185–200. https://doi.org/10.2343/geochemj.27.185.

Paonita, A., 2005. Noble gas solubility in silicate melts: a review of experimentation and theory, and implications regarding magma degassing processes. Ann. Geophys. 48 (4–5).
Pinti, D.L., Castro, M.C., Shouakar-Stash, O., Tremblay, A., Garduño, V.H., Hall, C.M., Hélie, J.F., Ghaleb, B., 2013. Evolution of the geothermal fluids at Los Azufres, Mexico, as traced by noble gas isotopes, δ18O, δD, δ13C and 87Sr/86Sr. J. Volcanol. Geoth. Res. 249, 1–11.
Pinti, D.L., Castro, M.C., López-Hernández, A., Hernández Hernández, M.A., Richard, L., Hall, C.M., Shouakar-Stash, O., Flores-Armenta, M., Rodríguez-Rodríguez, M.H., 2019. Cerro Prieto Geothermal Field (Baja California, Mexico) – a fossil system? Insights from a noble gas study. J. Volcanol. Geoth. Res. 371, 32–45.
Pinti, D.L., Haut-Labourdette, M., Poirier, A., Saby, M., van Hinsberg, V.J., Berlo, K., Castro, M.C., Gautason, B., Sigurðardóttir, Á.K., 2022. 87Sr/86Sr ratios and atmospheric noble gases in Theistareykir geothermal fluids: a record of glacial water. Geosciences 12, 119. https://doi.org/10.3390/geosciences12030119.
Poreda, R.J., Arnórsson, S., 1992. Helium isotopes in Icelandic geothermal systems: II. Helium-heat relationships. Geochim. Cosmochim. Acta. 56, 4229–4235.
Reeves, E.P., Seewald, J.S., Saccocia, P., Bach, W., Craddock, P.R., Shanks, W.C., Sylva, S. P., Walsh, E., Pichler, T., Rosner, M., 2011. Geochemistry of hydrothermal fluids from the PACMANUS, Northeast Pual and Vienna Woods hydrothermal fields, Manus basin, Papua New Guinea. Geochim. Cosmochim. Acta. 75 (4), 1088–1123.
Saby, M., Pinti, D.L., van Hinsberg, V., Gautason, B., Sigurðardóttir, Á., Castro, M.C., Hall, C., Óskarsson, F., Rocher, O., Hélie, J.-F., Mejean, P., 2020. Sources and transport of fluid and heat at the newly-developed Theistareykir Geothermal Field, Iceland. J. Volcanol. Geoth. Res. 405, 107062. https://doi.org/10.1016/j.jvolgeores.2020.107062.
Saby, M., van Hinsberg, V., Pinti, D.L., Berlo, K., Gautason, B., Sigurðardóttir, Á., Brown, K., Rocher, O., 2022. The behaviour of metals in deep fluids of NE Iceland. Sci. Rep. 12 (1), 21952.
Saemundsson, K., 2007. The geology of Theistareykir. Iceland GeoSurvey, Short Report ÍSOR-07270, p. 23 (in Icelandic).
Sano, Y., Fischer, T.P., 2013. The analysis and interpretation of noble gases in modern hydrothermal systems. The Noble Gases as Geochemical Tracers. P. Burnard. Springer Berlin Heidelberg, Berlin, Heidelberg, pp. 249–317.
Sano, Y., Wakita, H., 1985. Geographical distribution of 3He/4He ratios in Japan: implications for arc tectonics and incipient magmatism. J. Geophys. Res. 90, 8729–8741.
Seward, T.M., Williams-Jones, A.E., Migdisov, A.A., 2014. The Chemistry of Metal Transport and Deposition by Ore-Forming Hydrothermal Fluids, pp. 29–57.
Shanks, W.C., Thurston, R., 2012. Volcanogenic Massive Sulfide Occurrence Model. US Department of the Interior, US Geological Survey.
Sillitoe, R.H., 2010. Porphyry copper systems. Econ. Geol. 105 (1), 3.
Simmons, S.F., Brown, K.L., 2006. Gold in magmatic hydrothermal solutions and the rapid formation of a giant ore deposit. Science 314 (5797), 288–291.
Simmons, S.F., Sawkins, F., Schlutter, D., 1987. Mantle-derived helium in two Peruvian hydrothermal ore deposits. Nature 329 (6138), 429–432.
Simmons, S.F., Brown, K.L., Browne, P.R.L., Rowland, J.V., 2016. Gold and silver resources in Taupo Volcanic Zone geothermal systems. Geothermics 59, 205–214.
Stefánsson, A., Hilton, D., Sveinbjörnsdóttir, Á.E., Torsander, P., Heinemeier, J., Barnes, J.D., Ono, S., Halldórsson, S.A., Fiebig, J., Arnórsson, S., 2017. Isotope systematics of Icelandic thermal fluids. J. Volcanol. Geoth. Res. 337, 146–164.
Stracke, A., Zindler, A., Salters, V.J.M., McKenzie, D., Blichert-Toft, J., Albarède, F., Grönvold, K., 2003. Theistareykir revisited. G-cubed 4 (2).
Stuart, F.M., Burnard, P.G., Taylor, R.P., Turner, G., 1995. Resolving mantle and crustal contributions to ancient hydrothermal fluids: He-Ar isotopes in fluid inclusions from Dae Hwa W-Mo mineralisation, South Korea. Geochim. Cosmochim. Acta. 59 (22), 4663–4673.
Stuart, F.M., Lass-Evans, S., Godfrey, Fitton J., Ellam, R.M., 2003. High 3He/4He ratios in picritic basalts from Baffin Island and the role of a mixed reservoir in mantle plumes. Nature 424 (6944), 57–59.
Sun, W., Arculus, R.J., Kamenetsky, V.S., Binns, R.A., 2004. Release of gold-bearing fluids in convergent margin magmas prompted by magnetite crystallization. Nature 431 (7011), 975–978.
Sveinbjörnsdóttir, Á., Ármannsson, H., Ólafsson, M., Óskarsson, F., Markússon, S., Magnusdottir, S., 2013. The Theistareykir geothermal field, NE Iceland. Isotopic characteristics and origin of circulating fluids. Proc. Earth. Planet. Sci. 7, 822–825.
Sveinbjörnsdóttir, Á.E., Ármannsson, H., Óskarsson, F., Ólafsson, M., Sigurdardóttir, Á. K., 2015. A conceptual hydrological model of the thermal areas within the Northern neovolcanic zone, Iceland using stable water isotopes. Proc. World Geother. Congr. 2015, 1–7.
Symonds, R.B., Rose, W.I., Reed, M.H., Lichte, F.E., Finnegan, D.L., 1987. Volatilization, transport and sublimation of metallic and non-metallic elements in high temperature gases at Merapi Volcano, Indonesia. Geochem. Cosmochim. Acta 51 (8), 2083–2101.
Tardani, D., Tassara, S., Sanchez-Alfaro, P., Reich, M., Pérez-Flóres, P., Robidoux, P., Contreras, C., Pinti, D.L., Cembrano, J., Ague, J.J., 2024. The orientation of intra-arc crustal fault systems influences the copper budget of magmatic-hydrothermal fluids. Communications. Earth. Environ. 5 (1), 477. https://doi.org/10.1038/s43247-024-01629-8.
Tivey, M.K., 2007. Generation of seafloor hydrothermal vent fluids and associated mineral deposits. Oceanography 20 (1), 50–65.
Torgersen, T., Jenkins, W., 1982. Helium isotopes in geothermal systems: Iceland, the geysers, raft river and steamboat springs. Geochim. Cosmochim. Acta. 46, 739–748.
Tosdal, R.M., Dilles, J.H., Cooke, D.R., 2009. From source to sinks in auriferous magmatic-hydrothermal porphyry and epithermal deposits. Elements 5 (5), 289–295.
van Hinsberg, V., Vigouroux, N., Palmer, S., Berlo, K., Mauri, G., Williams-Jones, A., et al., 2017. Element Flux to the Environment of the Passively Degassing Crater Lake-Hosting Kawah Ijen Volcano, Indonesia, and Implications for Estimates of the Global Volcanic Flux. Geological Society London Special Publications, pp. 1–26. https://doi.org/10.6084/m9.figshare.c.2134359.
Varekamp, J.C., Ouimette, A.P., Herman, S.W., Bermúdez, A., Delpino, D., 2001. Hydrothermal element fluxes from Copahue, Argentina: a “beehive” volcano in turmoil. Geology. 29 (11), 1059. https://doi.org/10.1130/0091-7613(2001)029<1059:heffca>2.0.
Wahrenberger, C., Seward, T., Dietrich, V., 2002. Volatile Trace-Element Transport in High-Temperature Gases from Kudriavy Volcano (Iturup, Kurile Islands, Russia), vol. 7. Geochemical Society Special Publication, pp. 307–327.
Weiss, R.F., Lonsdale, P., Lupton, J.E., Bainbridge, A.E., Craig, H., 1977. Hydrothermal plumes in the galapagos rift. Nature 267, 600.
Weissberg, B.G., Browne, P.R., Seward, T.M., 1979. Ore metals in active geothermal systems. Geochemistry of Hydrothermal Ore Deposits, pp. 738–780.
Williams-Jones, A., Migdisov, A., 2014. Experimental Constraints on the Transport and Deposition of Metals in Ore-Forming Hydrothermal Systems, vol. 18. Society of Economic Geologists, pp. 77–96.
Williams-Jones, A.E., Migdisov, A.A., Archibald, S.M., Xiao, Z., 2002. Vapor-transport of ore metals. Water–Rock Interaction, Ore Deposits, and Environmental Geochemistry.: A Tribute to David A. Crerar. 279–306.
Witham, F., Blundy, J., Kohn, S.C., Lesne, P., Dixon, J., Churakov, S.V., Botcharnikov, R., 2012. SolEx: a model for mixed COHSCl-volatile solubilities and exsolved gas compositions in basalt. Comput. Geosci. 45, 87–97.
Wu, L.-Y., Hu, R.-Z., Li, X.-F., Stuart, F.M., Jiang, G.-H., Qi, Y.-Q., Zhu, J.-J., 2017. Mantle volatiles and heat contributions in high sulfidation epithermal deposit from the Zijinshan Cu-Au-Mo-Ag orefield, Fujian Province, China: evidence from He and Ar isotopes. Chem. Geol. 480, 58–65.
Yang, K., Scott, S.D., 2006. Magmatic fluids as a source of metals in seafloor hydrothermal systems. Back-arc spreading systems: geological, biological. Chemical, and Physical Interactions, pp. 163–184.
Yardley, B.W.D., Bodnar, R.J., 2014. Fluids in the continental crust. Geochem. Perspect. 3 (1), 1–127.
Zoller, W.H., Parrington, J.R., Phelan Kotra, J.M., 1983. Iridium enrichment in airborne particles from Kilauea volcano – january 1983. Science 222, 1118–1121.